Article

Cell Systems

Ultrasensitive molecular controllers for quasi-integral feedback

Graphical Abstract

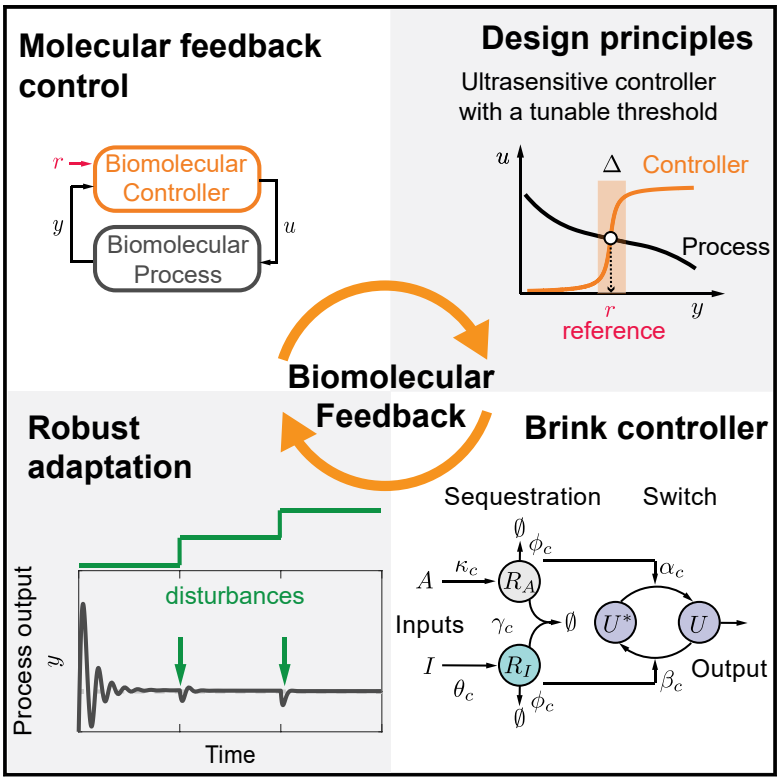

Highlights

- Feedback makes it possible to engineer adaptive biological systems
- We show that tunable ultrasensitive motifs can operate as robust feedback controllers
- We introduce and model the brink controller, a versatile ultrasensitive motif
- Our general feedback design principles are implementable through diverse mechanisms

Authors

Christian Cuba Samaniego, Elisa Franco

Correspondence

efranco@seas.ucla.edu

In Brief

Molecular feedback loops enable adaptive and dynamic behaviors in biology. Through computations and theory, we show that ultrasensitive motifs with a tunable threshold can operate as robust feedback controllers, and we suggest specific routes for practical implementation.

Cuba Samaniego & Franco, 2021, Cell Systems *12*, 272–288
March 17, 2021
https://doi.org/10.1016/j.cels.2021.01.001

CellPress

CellPress

Cell Systems

Article

Ultrasensitive molecular controllers for quasi-integral feedback

Christian Cuba Samaniego[1] and Elisa Franco[1,2,3,4,5,*]

[1]Mechanical and Aerospace Engineering, University of California at Los Angeles, Los Angeles, CA 90095, USA
[2]Molecular Biology Institute, University of California at Los Angeles, Los Angeles, CA 90095, USA
[3]Bioengineering, University of California at Los Angeles, Los Angeles, CA 90095, USA
[4]Mechanical Engineering, University of California at Riverside, Riverside, CA 92521, USA
[5]Lead contact
*Correspondence: efranco@seas.ucla.edu
https://doi.org/10.1016/j.cels.2021.01.001

SUMMARY

Feedback control has enabled the success of automated technologies by mitigating the effects of variability, unknown disturbances, and noise. While it is known that biological feedback loops reduce the impact of noise and help shape kinetic responses, many questions remain about how to design molecular integral controllers. Here, we propose a modular strategy to build molecular quasi-integral feedback controllers, which involves following two design principles. The first principle is to utilize an ultrasensitive response, which determines the gain of the controller and influences the steady-state error. The second is to use a tunable threshold of the ultrasensitive response, which determines the equilibrium point of the system. We describe a reaction network, named brink controller, that satisfies these conditions by combining molecular sequestration and an activation/deactivation cycle. With computational models, we examine potential biological implementations of brink controllers, and we illustrate different example applications.

INTRODUCTION

Feedback control enables the operation of most automated systems, from laptops to self-driving cars. Feedback works with the use of a rationally designed controller to reduce the discrepancy between the actual and desired behavior (reference or set point) of the process to be automated (Figure 1A). For example, a car cruise control system measures the speed of the vehicle, compares it to the reference speed, and modulates the fuel injection to reduce the error (fuel injection is increased if the speed is lower than the reference, or decreased if the speed is higher). This architecture provides two key advantages: (1) robustness: the process can maintain its reference in the presence of disturbances (for example, changes in the slope of the road) or uncertainty in the process parameters (for example, the number of passengers may not be known); (2) response design: the steady state and the response time of the automated system can be tuned (both the car speed and acceleration can be changed). Robustness and response design are obtained exclusively by updating the controller, without having to modify the process itself (Figure 1B) (Doyle et al., 1992; Åström and Murray, 2010). Feedback control of gene expression has been successfully implemented to achieve both classes of behaviors (robustness and response design), in applications that range from regulation of cell density to biofuel production (You et al., 2004; Kemmer et al., 2010; Siu et al., 2018). Most of these artificial feedback control systems are built using transcription factors, and they can be tuned to design the steady state or the kinetics of the closed-loop system (for instance, by varying promoter strength, ribosome-binding sites, or half-life of the repressor). However, their performance deteriorates in the presence of disturbances or if the parameters of the process are uncertain, such as with proportional controllers in engineering applications (Figure 1B) (Briat et al., 2016a).

In contrast, many complex natural pathways such as chemotaxis, the osmotic response, and even many electrophysiological processes have the capacity to maintain a set point in the presence of uncertainty and disturbances, thanks to the presence of an integrator in the system (Yi et al., 2000; Muzzey et al., 2009; De Palo et al., 2013). Similarly, industrial systems use integral controllers (the control input is proportional to the integral of the error) to guarantee that the system's output matches the desired reference (zero steady-state error) and that disturbances are rejected, a performance that cannot be achieved with proportional controllers (Figure 1B) (Åström and Murray, 2010). These observations have spurred the development of synthetic molecular controllers that operate as integrators, with particular focus on the use of molecular sequestration as a mechanism for reference setting (Briat et al., 2016a, 2016b; Olsman et al., 2019; Agrawal et al., 2018; Qian and Del Vecchio, 2018).

Sequestration-based controllers have been demonstrated experimentally, using sigma and anti-sigma factors and RNA molecules in *E. coli* or cell-free extracts (Huang et al., 2018; Aoki et al., 2019; Agrawal et al., 2019; Shannon et al., 2020). These results build on ample evidence that sequestration is suited to building robust feedback systems, with implementations that include nucleic acid networks *in vitro* (Franco et al.,

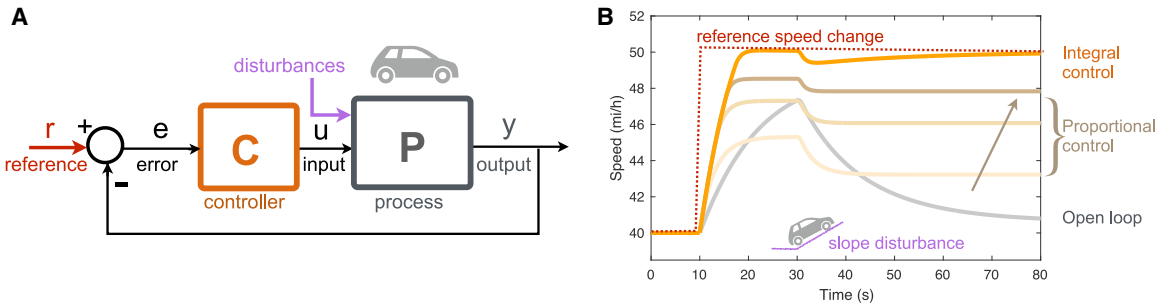

Figure 1. Feedback control enables reference tracking, adaptation, and design of the kinetic response

(A) Block diagram of a car cruise control system, in which the actual velocity (output *y*) is compared with the reference velocity and their difference is minimized as the controller computes the control variable *u*.

(B) Example simulations of a car cruise control system. A high gain proportional controller, which computes the control variable *u* as a linear function of the error, operates well, but cannot match an integral controller when it comes to reference tracking and disturbance rejection (MATLAB Simulink model from Åström and Murray, 2010).

2014), protein networks (Nevozhay et al., 2009; Hsiao et al., 2015; Annunziata et al., 2017; Shopera et al., 2017), and RNA regulators (Bloom et al., 2015; Kelly et al., 2018; Lillacci et al., 2018). Because a key feature of molecular sequestration is that it can yield a tunable ultrasensitive response (Buchler and Louis, 2008), the question arose as whether ultrasensitivity per se is a key property in building an integral molecular controller. Ultrasensitivity is common in biology, and it is an appealing design specification because it can naturally occur through the interconnection of distinct modules that do not need laborious tuning (Zhang et al., 2013).

Here, we examine ultrasensitive molecular components as candidate controllers to track a reference with zero or nearly zero error and achieve integral or quasi-integral action. We argue that this is possible as long as the ultrasensitive input-output map of the controller has a tunable threshold, which determines the reference to be tracked, and a tunable gain, which determines the steady-state error. This clear distinction in the roles of threshold and gain of the controller facilitates its design in isolation. Ultrasensitivity should be robust with respect to variations of the parameters and to the presence of downstream components, so that the performance of the controller is not compromised by uncertain operation conditions. We introduce a reaction network, named brink controller (BC), that exhibits all these properties: the motif combines molecular sequestration with an activation/deactivation cycle and presents a response akin to zero-order ultrasensitivity without operating in a saturated regime (Ferrell and Ha, 2014). Sequestration makes it possible to set the response threshold, and its combination with both an activation and a deactivation cycles improves ultrasensitivity. We show that under realistic parameter conditions the BC operates as a quasi-integral controller, as long as its response is ultrasensitive. We provide computational application examples where diverse implementations of the BC are used to regulate an *in vitro* network and a gene expression process.

RESULTS

Throughout the manuscript, we indicate chemical species with capital letters (e.g., *A*) and their concentration with the corresponding lowercase letters (e.g., *a*).

Design principles for quasi-integral molecular feedback control

The general architecture of a closed-loop biomolecular feedback system is shown in Figure 2A. Two subsystems, a biomolecular controller (*C*) and a biomolecular process (*P*), are interconnected via species *U* and *Y*, forming a negative feedback loop. In the presence of an integral controller, the concentration of the output of the biomolecular process *Y* should be identical to the concentration of the reference species *R*. To achieve quasi-integral performance at steady state, we propose the strategy illustrated in Figure 2B. First, the input-output steady-state maps of the controller (orange line $k_u(y, q, r)$, where *q* represents the controller parameters) and of the process (black line $k_y(u, p)$, where *p* represents the process parameters) are required to intersect at a single point, which is the only admissible steady state of the closed-loop system. Second, the controller input-output map should be ultrasensitive, i.e., the controller steady-state output concentration should increase steeply when its input is larger than a certain threshold. If the controller output response is ultrasensitive and its threshold is set by the reference species concentration *r*, then the steady state of the closed-loop system must fall in a neighborhood of *r*: the more ultrasensitive the controller response, the closer the steady-state *y* is to the reference *r*. Even if the process input-output map is uncertain or affected by perturbations (gray area), the closed-loop equilibrium is guaranteed to be close to the desired reference, as long as the controller is not operating in the saturated regime ($u \ll r$ or $u \gg r$). This simple architecture should yield a robust closed-loop system that (1) tracks changes in the reference input *r* (which determines the controller threshold) and (2) handles uncertainty and rejects perturbations on the process parameters. Ideally, the controller input-output map should also be robust with respect to parameter variations and to the presence of unmodeled or undesired reactions. Ultrasensitivity guarantees that the closed-loop equilibrium approaches the reference in the presence of perturbations: by increasing the steepness of the controller transition (yellow shaded area, $\Delta_{max}(u, q)$) we can decrease the steady-state error. In the ultrasensitive region, the steepness of the controller may be empirically approximated with a linear gain (blue line). Zero

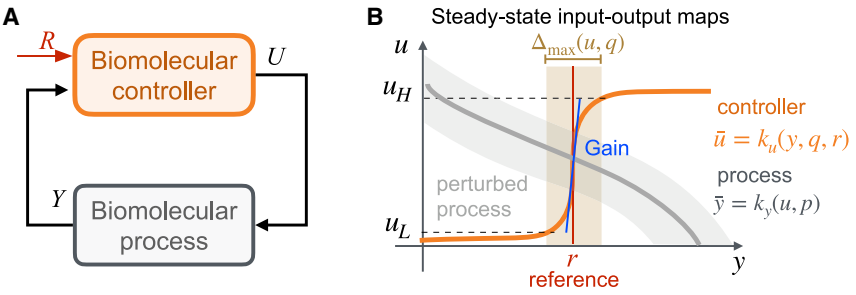

Figure 2. An ultrasensitive controller ensures robust closed-loop performance

(A) General architecture of a closed-loop molecular system including the target system to be controlled and the controller module.

(B) The output equilibrium of the closed-loop system is determined by the intersection of the steady-state maps of the controller (orange) $k_u(y,q,r)$, and of the process (dark gray), $k_y(u,p)$; q and p represent parameters characterizing, respectively, the controller and process. Ultrasensitivity of the controller guarantees that the equilibrium falls in a neighborhood of the threshold or reference (r). The error between the equilibrium and the reference can be characterized by the transition region $\Delta_{max}(u,q)$ (yellow shaded area) that depends on the controller parameters q; the width of the transition region is related to the steepness of the map, which can be locally described by a linear approximation or gain (blue line). A high controller gain makes it possible for the equilibrium to remain near the reference even when the process steady-state map is uncertain or subject to perturbations in the parameter vector p (gray-shaded area).

steady-state error could be achieved in the limit if the controller map is a step function. At the same time, because a steep ultrasensitive response may generate instability or oscillations within a negative feedback loop (Kholodenko, 2000), one must check that the steady state of the system's output y converges to r and returns to r in the presence of temporal perturbations (disturbances). The STAR methods provides additional details on our approach.

Many molecular networks, artificial and native, exhibit an ultrasensitive response (overview in Box 1). However, the threshold and the steepness of the steady-state map of most of these networks are difficult to tune. Because in our approach the threshold of the ultrasensitive controller must be determined by the reference for the process, any implementation should make it possible to vary the threshold over time as a function of an input signal or concentration. We next describe a network motif that satisfies this requirement by combining molecular sequestration with an activation/deactivation cycle.

The brink controller achieves a tunable, ultrasensitive input-output static map

Brink controller model

We describe an ultrasensitive synthetic molecular network that we named "brink" controller (BC) because of its steep, tunable steady-state response map (Figure 3A). The motif has two inputs, an activator species, A, and an inhibitor species, I, which respectively control the activation and deactivation of downstream species U, the output of the motif. We begin by assuming that the total concentration of output U remains constant, while it can either be in active (U) or inactive state (U^*). This simplification is acceptable if fluctuations of the total output concentrations are negligible or occur slowly relative to the other species in the system; the scenario with non-conserved output mass is examined later. The inhibitor I produces species R_I, which binds to and inhibits U by forming the inactive complex U^*. The activator A produces species R_A, which reactivates U^* by removing R_I from the complex U^*, thereby converting U^* back to U. Species R_A and R_I bind to each other (molecular sequestration) to produce a waste complex that does not interfere with the rest of the circuit. In addition, R_A and R_I degrade at a first order rate. The list of reactions is:

$$A \xrightarrow{\kappa_c} A + R_A,\ I \xrightarrow{\theta_c} I + R_I \text{ Production}$$

$$R_A + R_I \xrightarrow{\gamma_c} R_A \cdot R_I \text{ Sequestration}$$

$$R_A \xrightarrow{\phi_c} 0,\ R_I \xrightarrow{\phi_c} 0 \text{ Degradation and dilution}$$

$$R_A + U^* \xrightarrow{\alpha_c} U + R_A \cdot R_I \text{ Activation}$$

$$R_I + U \xrightarrow{\beta_c} U^* \text{ Deactivation}$$

Using the law of mass action, from these reactions we obtain an ordinary differential equation (ODE) model for the BC:

$$\dot{r}_A = \kappa_c a - \alpha_c r_A u^* - \gamma_c r_A r_I - \phi_c r_A, \qquad \text{(Equation 1)}$$

$$\dot{r}_I = \theta_c i - \beta_c r_I u - \gamma_c r_A r_I - \phi_c r_I, \qquad \text{(Equation 2)}$$

$$\dot{u} = \alpha_c r_A u^* - \beta_c r_I u, \qquad \text{(Equation 3)}$$

where i and a are inputs, and u and $u^* = u^{tot} - u$ are outputs. The model of the BC is a monotone system (Angeli and Sontag, 2003) and is unconditionally stable (see also STAR methods). These properties are shown to hold in Propositions 2–4 in the Section S3.

Within the BC two subsystems can be identified: a sequestration reaction and a switch (Figure 3A). The molecular sequestration (or titration) reaction operates like a comparator and ensures that only the most abundant species between I and A has a prevalent regulatory effect on U (Figure 3B, left). The switch reactions shift the balance between U and U^*, depending on the outputs of the comparator subsystem (Figure 3B) and increases ultrasensitivity (See also "Sequestration enables error computation in the brink controller, and activation/deactivation increase the gain," where we also briefly discuss the operation of the motif in a stochastic regime). To track a constant reference, the input operating as a reference (I or A) remains constant, whereas the other is allowed to vary over time. Note that the reference may also vary in time, as long as it varies more slowly than the timescale of convergence of the controller. When the BC is used within a feedback loop, the species maintaining constant or slowly varying concentration operates as the reference signal, while the time-varying species is the output of the process to be controlled.

Box 1. Ultrasensitivity: its implementations and implications

Ultrasensitivity occurs when the steady-state output of a molecular pathway increases rapidly once the input exceeds a certain threshold. This behavior can be achieved with four classes of mechanisms: (1) cooperativity, (2) molecular sequestration, (3) zero-order reactions (covalent modification cycles), and (4) on-off switching. We report a scalar ODE model for each mechanism, and we compute the maximum output static gain G, i.e., the maximum achievable slope of the steady-state input/output response (Zhang et al., 2013).

(1) Cooperativity is the result of binding-dissociation reactions of multiple molecules at equilibrium, and it is quantified by the cooperativity (Hill) coefficient n (Zhang et al., 2013; Ferrell, 2009). In a process regulated cooperatively by its input (see equations above), the output static gain G is proportional to the output production rate parameter κ and the input cooperativity coefficient n, and it is inversely proportional to the degradation rate parameter ϕ and the apparent dissociation constant K_d. The gain G could be increased by cascading cooperative modules which yield a higher Hill coefficient n. However, this increases the system complexity and worsens noise propagation (Hooshangi et al., 2005). The response threshold of cooperative modules K_d is also difficult to tune because molecular association-dissociation rates are not easily modified.

(2) Molecular sequestration can generate an ultrasensitive response via stoichiometric interactions (Buchler and Louis, 2008; Cuba Samaniego et al., 2016; Cuba Samaniego and Franco, 2017b). In the example above, the gain G is proportional to the production rate constant κ and inversely proportional to the degradation/dilution parameter ϕ of the components (Section S2.2). The input concentration w determines the threshold of ultrasensitivity, which is therefore easily tuned. In the absence of degradation (ϕ=0) the system will produce an infinite gain G, yielding perfect integral action, as proposed in the molecular sequestration controller (MSC) (Briat et al., 2016a; Qian and Del Vecchio, 2018). Timescale separation arguments make it possible to overcome the influence of ϕ (Qian and Del Vecchio, 2018). However, experimental characterization of molecular sequestration processes *in vivo* and *in vitro* suggest that it is difficult to achieve a high static gain on a non-logarithmic scale (Buchler and Cross, 2009; Ricci et al., 2011).

(3) Zero-order ultrasensitivity occurs when enzymes operate in a regime of saturation. This creates a higher gain than molecular sequestration, and it requires saturation of enzymes. The static gain of this example module has been computed (Goldbeter and Koshland, 1981; Del Vecchio and Murray, 2015). The input w can be used to easily tune the output response threshold. A push-pull motif of a covalent modification cycle was reported to achieve zero-order ultrasensitivity *in vitro* (Kajita et al., 2017), although this behavior is hard to find in nature (Goldbeter and Koshland, 1981). This mechanism satisfies the requirements discussed here for quasi-integral action (ultrasensitivity and tunable threshold). However, ultrasensitivity is compromised when the circuit is connected to a downstream process (Del Vecchio and Murray, 2015).

(4) Systems with a nearly digital on-off behavior achieve a nearly infinite static gain, as there is a sharp transition between two steady states. This behavior can be achieved with bistable switches; however, the switching threshold usually depends on a combination of the network parameters and may be difficult to tune (Zhang et al., 2013). A recombinase protein switch was used to obtain a sharp output transition with nearly infinite gain (Siuti et al., 2013; Bonnet et al., 2012; Folliard et al., 2017). In this system, however, the threshold is difficult to tune as it depends on the dissociation constant of protein-DNA interaction. In addition to being difficult to tune, thresholds may also be asymmetric and depend on the switching direction (hysteresis).

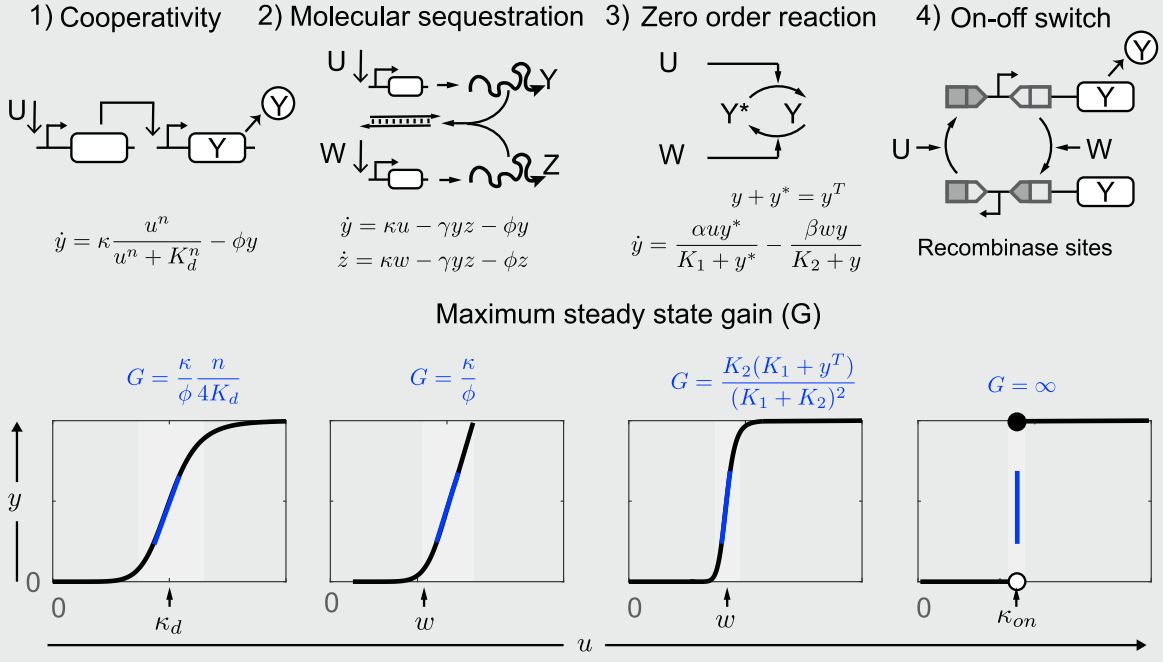

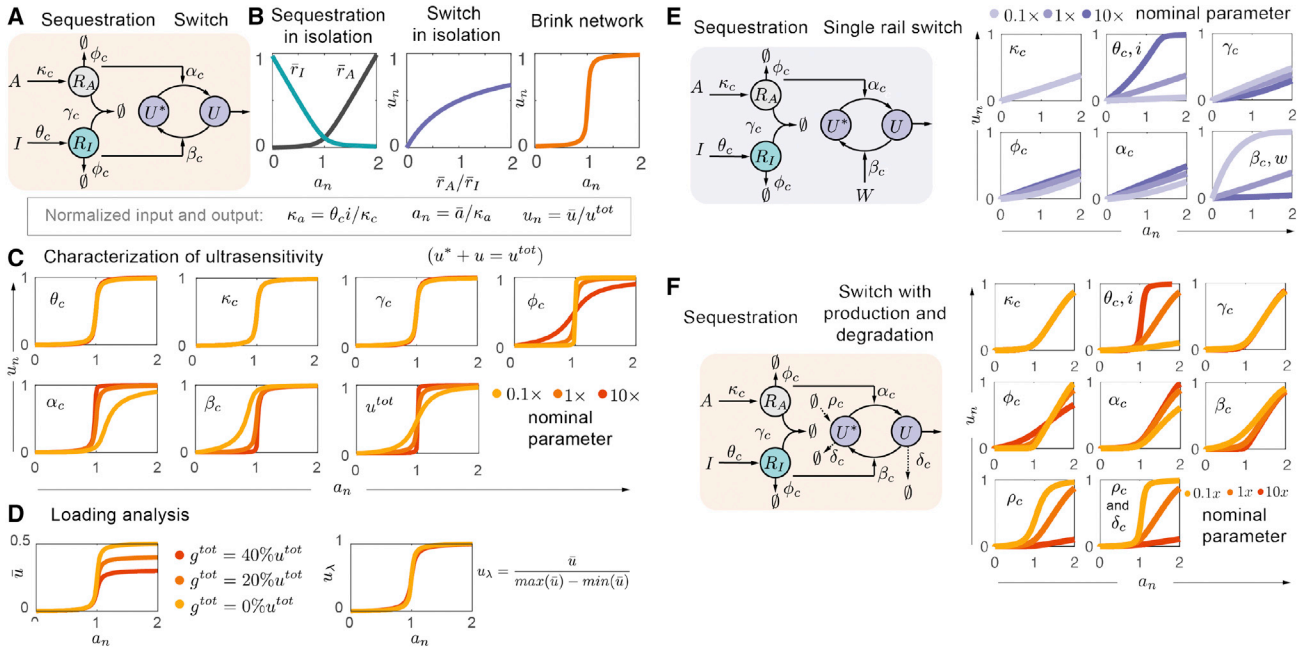

Figure 3. The brink controller (BC) combines sequestration with an activation/deactivation cycle to achieve a tunable ultrasensitive input-output map

(A) Summary of the reactions defining the BC. The inputs of the controller are species A (activator) and species I (inhibitor). The output of the controller is species U.

(B) Example simulation of the steady-state input-output map of the sequestration and switch reactions in isolation (left and central panel) and when they are interconnected (right panel). Here, the concentration of input I is fixed, while the concentration of input A varies. The equilibrium concentration of A, $\bar{a}$, is normalized with respect to the threshold constant $k_a(i)$, and the equilibrium concentration of U, $\bar{u}$, is normalized with respect to its total concentration u^{tot}.

(C) Computational analysis of the steady-state input-output map of the motif: in each subplot a single parameter is varied, while all other parameters remain constant (nominal values in Table 1).

(D) If the controller output u binds to a downstream load g, there is a reduction of the available free output at equilibrium $\bar{u}$ (left), according to expression (Equation 8). Here, we consider the worst-case scenario in with dissociation constant $\kappa_M = 0$ (irreversible binding and consumption of u). Ultrasensitivity of the BC is however robust to the presence of a load, which is evident if we normalize $\bar{u}$ with respect to the total output range (right). Figure S3 shows the effects of a load up to 80% of u^{tot}.

(E) Schematic of a variant of the BC in which only the activation cycle is regulated, while deactivation is controlled by an additional input species, W; here we assume w = 0.025 μM, i = 0.4 μM. On the right, we compute the normalized steady-state response of this "single-rail" BC as individual parameters are changed relative to their nominal values. The loss of one branch of regulation of the switch results in a reduced ultrasensitivity. All input-output maps shown here are derived in Section S3.

(F) Simulation of the input-output map in the presence of production and degradation of the output species. Ultrasensitivity is reduced significantly, unless the production and degradation rate constants are sufficiently small. We assumed nominal $\delta_c = \phi_c$, $\rho_c = 0.5\delta_c$, and i = 0.4 μM. At lower values of δ_c, the reduction of ultrasensitivity is moderate (plots in Figure S3). Unless otherwise noted, the nominal reaction parameters used in all these simulations are listed in Table 1.

Ultrasensitivity conditions at steady state

Here, we derive expressions for the input-output static map of the BC, and we obtain analytical conditions which guarantee ultrasensitivity of the map.

First, we consider the case in which *I* is kept constant and acts as a reference input to the module, while *A* can vary. We derive equilibrium conditions by setting Equations 1, 2, 3 equal to zero. Finding the controller output *u* as a function of *a* and *i* is a long and tedious procedure, however, *a* can be expressed more easily as a function of *i* and *u* in closed form (Section S3.3). Subtraction of Equations 1 and 2 (with Equation 3 at equilibrium) yields the steady-state $\bar{a}$:

$$\bar{a} = \frac{\theta_c}{\kappa_c} i + \frac{\phi_c}{\kappa_c}\left(\bar{r}_A - \bar{r}_I\right). \qquad \text{(Equation 4)}$$

By substituting the equilibrium expressions for $\bar{r}_A$ and $\bar{r}_I$ as a function of the input *i* and $\bar{u}$ (Section S3.3) we can rewrite Equation 4 as:

$$\bar{a}(\bar{u}, i) = k_a(i) + \Delta(\bar{u}, i), \qquad \text{(Equation 5)}$$

with $k_a(i) = \frac{\theta_c}{\kappa_c} i$ being the normalized reference and $\Delta(\bar{u}, i) = \frac{\phi_c}{\kappa_c}\left(1 - \frac{\alpha_c \bar{u}^*}{\beta_c \bar{u}}\right)\bar{r}_A(\bar{u}, i)$. Expression (Equation 5) is useful because it allows for breaking down $\bar{a}(\bar{u}, i)$ as the sum of a threshold $k_a(i)$ depending on input *i*, and of an additional term $\Delta(\bar{u}, i)$ (compare with Figure 2B). The presence of basal production (leak) of species R_A and R_I affects expression (Equation 5) by introducing a bias that shifts the threshold (Section S3.7).

Are there parametric conditions that make the input-output static map ($\bar{u}$ versus $\bar{a}$) ultrasensitive? This question can

Table 1. Nominal simulation parameters used for the BC and the protein expression process

Rate	Description	Value	Other studies
θ_c (/s)	production	$5{\cdot}10^{-4}$	$[10^{-4}, 1]$ (Milo and Phillips, 2015; Qian and Del Vecchio, 2018; Chen et al., 2015)
κ_c (/s)		$5{\cdot}10^{-4}$	$[10^{-4}, 1]$
γ_c (/M/s)	sequestration	$3{\cdot}10^{4}$	$[10^{4}, 10^{6}]$ (Kim et al., 2006; Zhang et al., 2007; Qian and Del Vecchio, 2018)
ϕ_c (/s)	degradation	$3.85{\cdot}10^{-4}$	$[10^{-4}, 10^{-3}]$ (Kim et al., 2014; Qian and Del Vecchio, 2018)
α_c (/M/s)	activation	$1.2{\cdot}10^{5}$	$[10^{4}, 10^{6}]$ (Lloyd et al., 2018)
β_c (/M/s)	deactivation	$1.2{\cdot}10^{5}$	$[10^{4}, 10^{6}]$
$\delta_c = \phi_c$ (/s)	degradation	–	–
$\rho_c = 0.5\delta_c$ (M/s)	production	–	–
κ_s (*nM*)	dissociation	200	–
α_s (/ s)	production	$1{\cdot}10^{-3}$	$[10^{-4}, 1]$ (Milo and Phillips, 2015; Chen et al., 2015)
ψ_s (/s)		$9.6{\cdot}10^{-4}$	$[10^{-4}, 1]$
$\phi_s = \phi_c$ (/s)	degradation	–	–
$\delta_s = \phi_c$ (/s)	–	–	–
n_s	cooperativity	2	[1, 5]

be answered by noting that if the motif is ultrasensitive, small changes in *a* must correspond to large changes in *u* when $\bar{a} \approx k_a(i)$. Therefore, we focus on term $\Delta(\bar{u}, i)$, which is reduced when:

$$\frac{\beta_c}{\gamma_c}\bar{u} \gg 4\frac{\theta_c}{\alpha_c}\frac{i}{\bar{u}^*}. \qquad \text{(Equation 6)}$$

This condition (derived in Section S3.3) could be satisfied by multiple combinations of parameters. For example, a large sequestration constant γ_c goes hand in hand with large switching parameters α_c and β_c. Additionally, the term $\Delta(\bar{u}, i)$ is proportional to the ratio of degradation and production rate constants of r_A, ϕ_c/κ_c, with a small degradation rate constant ϕ_c promoting ultrasensitive behavior. In Section S3.8 we derive similar ultrasensitivity conditions, in which the production rates of R_A and R_I are nonlinear Hill-type rates that exhibit saturation, which may be more realistic in practice.

In summary, ultrasensitivity improves when the sequestration and activation/deactivation parameters are large. Additionally, the threshold of the ultrasensitive response, $\kappa_a = \frac{\theta_c}{\kappa_c} i$, can be tuned linearly with the input *i*. A slow degradation parameter ϕ_c also promotes utrasensitivity.

These derivations are supported by computations of expression (Equation 4) in Figure 3C (parameters are in Table 1). The x axis of this plot uses a threshold-normalized input $a_n = \frac{\bar{a}(u,i)}{\kappa_a}$. The nominal sequestration parameter γ_c and switching parameters α_c and β_c are chosen to be in a realistic range for nucleic acid and protein interactions and are on the same order of magnitude. Ultrasensitivity is not drastically affected if we change γ_c within one order of magnitude of the nominal value. However, variations of α_c and β_c in the same range make the transition less sharp. As predicted by the analytical approximation, a small degradation rate constant, ϕ_c, improves ultrasensitivity. Changes in θ_c and κ_c primarily affect the threshold κ_a, however, because our plot uses a threshold-normalized input these effects are not visible. In Section S3.3, we follow similar steps to find the input-output mapping when the inhibitor *i* is varied, while the activator *a* is constant and determines the threshold for the input-output map and obtain ultrasensitivity conditions consistent with those reported above.

The maximum slope of the input-output map, or gain, of the BC can be estimated as:

$$G_{max,BC} \approx \frac{1}{4}\frac{(u^{tot})^2}{\left(1+\frac{\alpha_c}{\beta_c}\right)}\frac{\alpha_c}{\phi_c\kappa_a(i)}, \qquad \text{(Equation 7)}$$

with $\kappa_a(i) = \frac{\theta_c}{\kappa_c} i$. This expression holds when the motif is activated by input *a*, while species *i* is held constant; a similar expression can be derived when *i* is constant and *a* varies (Section S3.5). The input-output steady-state map of the BC model can be approximated using a Hill Function that has the same threshold and maximum gain (Box 1 and Section S3.5).

The brink controller preserves ultrasensitivity in the presence of a downstream load

If the BC is used as a controller in a closed-loop system, its output, *U*, must operate as the input to other pathways. Thus, a fraction of *U* may be depleted as it participates in other reactions, which can be considered as a "load" that deteriorates performance through a phenomenon called retroactivity (Del Vecchio et al., 2008). Because the ability of the BC to achieve quasi-integral performance is determined exclusively by the ultrasensitivity of its steady-state input-output map, transient loading effects are not expected to matter. However, a load can change the input-output equilibrium conditions of the system (Franco et al., 2011). We illustrate this case with a model example (Section S3.6) in which the concentration of *U* is depleted by binding to a downstream promoter, *g*. In this case, the concentration balance of *u* becomes:

$$u^* = u^{tot} - u - \lambda,\ \lambda = \frac{u}{u+\kappa_M} g^{tot},\ \kappa_M = \frac{\kappa_{off}+\kappa_{cat}}{\kappa_{on}}. \qquad \text{(Equation 8)}$$

Term λ captures the loading effects at steady state, has a maximum value $\lambda = g^{tot}$, and decreases when the dissociation constant κ_M is large relative to u^{tot}.

At steady state the load depletes molecules of U, thereby reducing the free u as shown by the simulations in Figure 3D, left ($\kappa_M = 0$) and limiting the capacity of the controller to direct downstream processes. Similar effects occur if the load reaction is irreversible ($\kappa_{off} = 0$). However, upon normalizing relative to the maximum level of available u, ultrasensitivity of the map is robust with respect to the presence of load (Figures 3D, right, and S3). In other words, the controller is likely to perform well in terms of tracking and disturbance rejection, but there are limitations on the amount of load it can handle. If the concentration of the load is low, the loading effect is negligible, even in the presence of a strong binding site for U. For example, if U is a transcription factor and g is a binding site on the genome or on a low-copy plasmid, loading effects are unlikely to affect performance.

If U participates in a downstream catalytic process, then it may have a low average "occupancy" with negligible loading effects. For example, U may be, itself, a promoter site to which RNA polymerase binds to initiate mRNA transcription, or an mRNA species that binds to ribosomes and is translated into a protein. Because RNA polymerase and ribosomes only transiently occupy their binding sites, their loading contribution should be similar to Equation 8 with a very large κ_M. Most importantly, promoters and ribosome-binding sites can be designed to not overlap with regulatory domains, thus decoupling the ability of U to take part in the reactions of activation and deactivation from its ability to take part in downstream "actuation" reactions.

Direct regulation of both activation and deactivation improves ultrasensitivity

A salient feature of the BC is that the products of input species not only mutually sequester but also individually control activation and deactivation of the controller output. To clarify what the benefit of regulating both activation and deactivation is, in Section S3.9 we examined a model in which activation is controlled by R_A, while deactivation is controlled by an additional (constant) input. Because only one reaction of the cycle is influenced by the input, we refer to this case as a "single-rail" BC (Figure 3E). (The same analysis could be done for the case in which deactivation is regulated by R_I, while activation is regulated by W.) Using parameters consistent with those adopted for the BC (Table 1), we compute the single-rail BC equilibrium map in Figure 3E, where we examine the influence of changes in individual parameters. In this case ultrasensitivity is more difficult to achieve, it is more sensitive to parameter changes, and, unlike the BC, it depends also on the reference concentration i; this indicates that direct control of both activation and deactivation is key to support robust ultrasensitivity of the BC.

Production and degradation of the output species reduce ultrasensitivity

Most molecules in the cellular environment are dynamically produced and degraded, although their average level may be tightly regulated. Thus, the effects of production and degradation reactions of the output species U on the behavior of the BC are prime for examination. We consider, without loss of generality, the motif when the inhibitor input I is held constant. In this case, we assume that u^* (inactive output) is produced at a rate constant ρ_c and degraded with a rate constant δ_c, while the dynamics of r_A and r_I are unchanged:

$$\dot{u} = \alpha_c r_A u^* - \beta_c r_I u - \delta_c u, \qquad \text{(Equation 9)}$$

$$\dot{u}^* = \beta_c r_I u - \alpha_c r_A u^* + \rho_c - \delta_c u^*. \qquad \text{(Equation 10)}$$

Note that $u^{tot}(t) = u(t) + u^*(t)$, and $\dot{u}^{tot} = \rho_c - \delta_c u^{tot}$, whose equilibrium value is $\bar{u}^{tot} = \rho_c/\delta_c$. If production and degradation are slow, it is sensible to simply assume that $u^{tot} \approx \rho_c/\delta_c$. Yet, it is useful to derive the input-output map of the BC:

$$a(\bar{u}, i) = k_a(i) + \Delta(\bar{u}, i) + \varepsilon_1 \cdot (\bar{u} + \varepsilon_0), \qquad \text{(Equation 11)}$$

in which $k_a(i)$ and $\Delta(\bar{u}, i)$ are defined like the corresponding terms in expression (Equation 5), where now $\bar{u}$ is determined by both parameters δ_c and ρ_c. The new terms are $\varepsilon_0 = \phi_c/\beta_c$ and $\varepsilon_1 = \delta_c/\kappa_c$ (complete derivations are in Section S3.3). The motif can exhibit an ultrasensitive response when $\Delta(\bar{u}, i)$ is small. This is achieved when $\gamma_c \gg \phi_c$, $\alpha_c \gg \delta_c$, and $\frac{\beta_c}{\gamma_c}\bar{u} \gg 4\frac{\theta_c i + \delta_c \bar{u}}{\alpha_c \bar{u}^*}$, which can be satisfied if the switching rate constants β_c and α_c are large. While these requirements are similar to what was derived earlier, it should be noted that introducing production and degradation of the output results in a new term $\varepsilon_1 \cdot (\bar{u} + \varepsilon_0)$ in the input-output map. While ε_0 is negligible as long as β_c is large, the term $\varepsilon_1 \bar{u}$ can only be neglected if it is assumed that δ_c, the degradation rate constant of u, is sufficiently small relative to κ_c, the production rate constant of the activator. These analytical derivations do not provide direct insights into the effects of ρ_c, however, with computer simulations in Figure 3F, it is shown that $\delta_c = \phi_c$ and $\rho_c = \bar{u}^{tot}\delta_c$ ($\bar{u} = 0.5\,\mu M$) are sufficient to hamper ultrasensitivity of the controller. If the output production and degradation parameters are smaller, their influence on ultrasensitivity is less significant as shown in Section S3.3, Figure S4.

The brink controller as a quasi-integral feedback controller

We now consider the BC interconnected with a target process in a closed-loop system. Here, we assume that the closed-loop system is stable and that it has a monotonically increasing input-output static map, with the latter assumption guaranteeing uniqueness of the closed-loop equilibrium. We focus on two criteria to evaluate performance: the capacity of the closed-loop system to track changes in reference to small steady-state error and to reject perturbations of the process parameters. The BC is operated as a controller in which the activator input is a reference R, and the inhibitor input is interconnected to the process output Y and used as an inhibitor for the motif. This will result in the controller having an input-output map that is monotonically decreasing, guaranteeing that the feedback loop is negative. The output of the controller is U, which becomes the input for the

process. The dynamics of the interconnected controller and process are:

$$C\begin{cases} \dot{r}_r = \overbrace{\kappa_c r}^{\text{reference}} - \alpha_c r_r u^* - \gamma_c r_r r_y - \phi_c r_r, \\ \dot{r}_y = \overbrace{\theta_c y}^{\text{feedback}} - \beta_c r_y u - \gamma_c r_r r_y - \phi_c r_y, \\ \dot{u} = \alpha_c r_r u^* - \beta_c r_y u, \end{cases} \quad \text{(Equation 12)}$$

$$P\begin{cases} \dot{x} = f(x,u,p), \\ y = h(x), \end{cases} \quad \text{(Equation 13)}$$

with mass conservation $u^{tot} = u^* + u$. Like in Equation 5, the output of the process at steady state is:

$$\bar{y}(\bar{u},r) = k_r(r) + \Delta(\bar{u},r), \quad \text{(Equation 14)}$$

where $k_r(r) = \frac{\kappa_c}{\theta_c} r$ is the scaled reference and $\Delta(\bar{u}, r) = \frac{\phi_c}{\theta_c}\left(\frac{\beta_c \bar{u}}{\alpha_c \bar{u}^*} - 1\right)\bar{r}_y(\bar{u},r)$.

The brink controller operates as a quasi-integral controller near steady state

When the degradation rate constant ϕ_c is zero, we have $\Delta(\bar{u},r) = 0$, and thus:

$$\bar{y}(r) = k_r(r),$$

representing that the system exhibits perfect integral action. In this case, the closed-loop steady state of the output is equivalent to that achieved using a molecular sequestration controller (MSC) (Briat et al., 2016a). In some *in vitro* systems degradation can be eliminated or reduced, thus is reasonable to assume $\phi_c \approx 0$. In contrast, *in vivo* systems always present degradation and dilution thus $\phi_c > 0$ and $\Delta(\bar{u},r) \neq 0$. This phenomenon is also known as "leak" in the context of MSCs (Qian and Del Vecchio, 2018), and its effects can be mitigated by increasing production and sequestration parameters (Huang et al., 2018; Aoki et al., 2019) (Figure 4D). Similarly, this limitation can be mitigated in the BC by achieving ultrasensitivity: if the BC is ultrasensitive, then $\Delta(\bar{u}, r) \approx 0$, and therefore, it operates as a quasi-integral controller in a closed loop (Figure 4E). In Section S3.4, it is demonstrated that if the parameters of the BC satisfy the ultrasensitivity condition (Equation 6), then the input-output transfer function of the linearized system (near equilibrium) includes a pole at the origin in the Laplace domain. In turn, this means that the corresponding closed-loop system includes a zero at the origin and is therefore insensitive to step inputs. In other words, by performing quasi-integral action the BC confers to the closed-loop system the capacity to track a reference and to reject disturbances.

At the same time, loss of ultrasensitivity of the BC means a larger steady-state error. We have previously noted that ultrasensitivity is reduced if a single-rail architecture is adopted, or if the output is produced and degraded; in the latter case, the closed-loop Equation 14 is modified similarly to Equation 11, showing that a larger steady-state error is to be expected, and the quasi-integral performance is lost (see also Figure 4F).

The steady-state error of the closed-loop system is bounded

An approximation of the steady-state error can be derived from Equation 14:

$$\bar{e} = \Delta(\bar{u},r) = \frac{\phi_c}{\theta_c}\left(\frac{\beta_c \bar{u}}{\alpha_c \bar{u}^*} - 1\right)\bar{r}_y(\bar{u},r) = \frac{\phi_c}{\theta_c}\left(1 - \frac{\alpha_c \bar{u}^*}{\beta_c \bar{u}}\right)\bar{r}_r(\bar{u},y) \quad \text{(Equation 15)}$$

Assuming $\alpha_c = \beta_c$, from expression (Equation 15) we find a bound for the error when the equilibrium $\bar{u}$ is in the interval from $0.1u^{tot}$ to $0.9u^{tot}$. Recalling that $\bar{r}_y \approx \frac{k_c}{\beta_c}\frac{r}{u}$ (Section S3), we find:

$$|\bar{e}| < \frac{80}{9}\frac{\phi_c}{\beta_c u^{tot}} k_r(r),$$

where $k_r(r) = \frac{k_c}{\theta_c} r$. With the nominal parameters in Table 1, the error normalized to the scaled reference is $|\bar{e}|/k_r(r) < 3\%$. The above error bound can be related to the maximum gain expression (Equation 7):

$$|\bar{e}| < \frac{K}{G_{max,BC}}, \quad \text{(Equation 16)}$$

where K depends on the considered input interval and on the total output u^{tot}. This expression confirms that a high gain reduces the steady-state error.

Comparing the brink controller with a leaky molecular sequestration controller

Recent work has shown that sequestration alone can provide integral action, through what is known as MSC or antithetic controller (Briat et al., 2016a; Huang et al., 2018; Aoki et al., 2019). A well-known challenge for "exact" integral action is the presence of degradation and dilution of the sequestering species, which yield a "leaky" MSC (LMSC), shown in Figure 4A (Briat et al., 2016a; Qian and Del Vecchio, 2018; Aoki et al., 2019). This challenge can be illustrated referring to the sequestration reaction described in Box 1: if the leak parameter ϕ is large, the slope of the steady-state map (gain) decreases, and in the context of a stable closed-loop system this results in larger deviation from the reference (see schematic in Figure 2). In contrast, if ϕ is small, then the slope of the steady-state map becomes steep, yielding an infinite gain in the limit $\phi \to 0$, which has the effect of locking the closed-loop equilibrium at the reference value (for any value of production and sequestration constants). In the presence of leak, the gain of the LMSC can be improved by increasing the production rate parameters (Figure 4D); integral performance can also be recovered by tuning "both" production and sequestration parameters to operate the controller on a much faster timescale than the process (Huang et al., 2018). Here, we discuss how, as an alternative route, the adoption of a BC can mitigate requirements on production and sequestration parameters while still achieving quasi-integral feedback; we also highlight when this route fails.

We use computations to compare the LMSC (Figure 4A, left) and the BC (Figure 4A, middle) using consistent parameters.

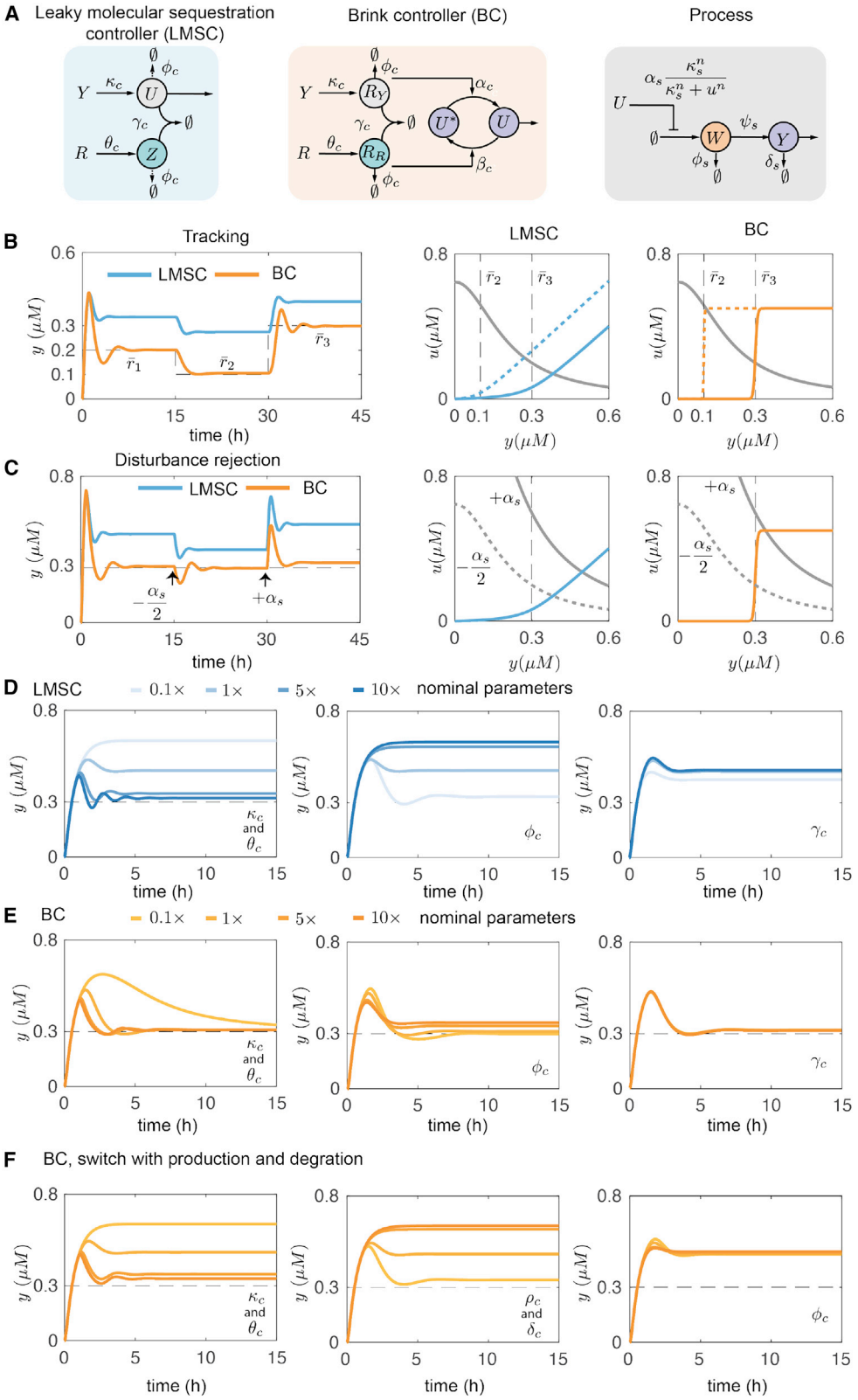

Figure 4. Closed-loop performance of the BC in comparison with a LMSC

(A) Schematics summarizing the reactions occurring in the LMSC, in the BC, and in the gene expression process.

(B) Left: comparison of reference tracking performance in a closed loop. Here, $\bar{r}_i$ is the scaled reference $\bar{r}_i = k_r(r_i)$ from Equation 14. This definition of rescaled reference is consistent with previous work on MSC controllers (Briat et al., 2016a; Qian and Del Vecchio, 2018). Right: equilibrium conditions of

(legend continued on next page)

Throughout Figure 4, orange/red traces refer to the BC, while cyan/blue traces refer to the LMSC. As an example model process, we consider expression of a target protein y (Figure 4A, right):

$$\dot{x} = \alpha_s \frac{\kappa_s^{n_s}}{\kappa_s^{n_s} + u^{n_s}} - \phi_s x \ (\textit{process dynamics}),$$
$$\dot{y} = \psi_s x - \delta_s y \ (\textit{process output}). \qquad \text{(Equation 17)}$$

The ODEs of each controller are reported in Section S3.9, and the nominal simulation parameters are listed in Table 1. A sequestration rate constant that is realistic for nucleic acids and proteins was selected, and the production and degradation rate parameters considered were comparable with those used in recent computational studies of the LMSC (Qian and Del Vecchio, 2018; Briat et al., 2016b) (see also Table S6).

First, with illustrative simulations in Figure 4B we show that in the presence of leak (half-life of about 30 min), the BC can track the reference very closely, while the LMSC produces a large steady-state error. The solutions to the ODEs (left) are shown as well as the equilibrium conditions (right), which highlight how shifting the reference results in a shift of the BC ultrasensitivity threshold. In Figure 4C, we compare the ability of these controllers to reject disturbances in the process parameters. We vary the transcription rate, α_s, which results in a change of the process equilibrium conditions (right, gray line). The BC maintains the desired reference, rejecting this disturbance, while the LMSC results in a steady-state offset. This difference in performance can be explained by comparing the gain of the LMSC, $G_{LMSC} = \kappa_c/\phi_c$, derived in Equation 21, with the maximum gain for the BC when $\alpha_c = \beta_c$, $G_{max,BC} \approx \frac{1}{8}\frac{(u^{tot})^2\beta_c}{\phi_c\kappa_r(r)}$, from Equation 7. Using the nominal values in Table 1, $G_{LMSC} \approx 1.3$, which is realistic for RNA-based LMSCs (Franco et al., 2014; Huang et al., 2018) in *E. coli*, where the half-life of mRNA is estimated between 3–30 min and production of mRNA is estimated between $0.02 - 0.1$/min (Golding et al., 2005; Shimoni et al., 2007). These figures yield $G_{LMSC} \approx 0.09 - 4$. In comparison, with the nominal parameters in Table 1, $G_{max,BC} \approx 97.6$ when $r = 0.1$ μM and $u^{tot} = 0.5$ μM, which are realistic concentrations for signaling molecules. Naturally, the gains of both LMSC and BC may be tuned by changing various parameters. For example, production parameters can be increased by improving promoter and RBS strength, as well as plasmid copy numbers; in mammalian cells, gains may be naturally higher due to the faster production rate (0.96–1.92/min Darzacq et al., 2007) and longer half-life (600 min) of mRNA.

Next, we vary individual parameters of LMSC and BC and examine their effect on the temporal response to a step change in reference (Figures 4D–4F). Both LMSC and BC respond faster when the production parameters κ_c and θ_c are large (both are varied simultaneously to preserve the scaled reference value); the steady-state tracking is improved in the LMSC but not significantly affected in the BC (consistent with Figure 3C). The performance of the BC is not very sensitive to changes in the degradation parameter ϕ_c; in contrast, when ϕ_c is large, the LMSC loses quasi-integral reference tracking. Both LMSC and BC are not very sensitive to changes of sequestration parameter γ_c. As discussed before, ultrasensitivity of the BC is compromised in the presence of production and degradation of the output species U (parameters ρ_c and δ_c, both varied simultaneously to preserve the equilibrium value $\bar{u}$), and this causes an increase of steady-state error comparable to that caused by large ϕ_c in the LMSC (Figure 4F); in this case the BC error can be reduced by increasing the production parameters κ_c and θ_c, but it is not eliminated by removing the leak parameter ϕ_c. The effects of changing other parameters on the equilibrium of the step response of the BC can be inferred from the plots in Figures 3C and 3F.

These simulations highlight the fact that the BC offers robustness to the presence of leak when compared with the LMSC with the same production and sequestration parameters, at the expense of increasing complexity by adding the activation/deactivation reactions of the output U. However, this advantage in robustness is lost when the total amount of U cannot be tightly regulated. In this case, a more convenient approach to maintain quasi-integral behavior is to simply increase the gain of the LMSC as much as possible, by increasing for example θ_c and κ_c. The influence of δ_c and ρ_c on the BC steady-state error appear to be similar to the influence of ϕ_c on the LMSC, but generally assuming $\delta_c = \rho_c = 0$ is not sufficient to achieve perfect integration because it does not guarantee ultrasensitivity; in contrast, taking $\phi_c = 0$ in the LMSC eliminates leak and yields a perfect integrator (MSC). (As noted before, also, the BC is a perfect integrator when $\phi_c = \delta_c = \rho_c = 0$, since it includes an MSC module.) Finally, while this analysis is centered around steady-state behavior, the simulations in Figure 4 indicate that the BC can generate an overshoot that is larger than the LMSC. This may be a disadvantage of the BC, as it yields an initial output production larger than needed. The response kinetics of the two controllers (time it takes to reach steady state) are generally comparable.

Application examples

We model three alternative implementation routes of the BC. We discuss how both RNA molecules and proteins may be

the controller (LMSC in cyan, BC in orange) and the process (gray); a change in reference shifts the ultrasensitive threshold of the BC, enabling reference tracking.

(C) Left: comparison of disturbance rejection performance. Right: equilibrium conditions. The process steady-state map changes with variations in the process parameter (α_s is taken as an example); however, in the presence of the BC the equilibrium point remains near the reference value.

(D and E) Temporal behavior of the output step response y as a single parameter of the LMSC (D, blue traces) or BC (E, orange traces) is varied with respect to the nominal values. Increasing the production parameters improves reference tracking in both controllers, as their gain is increased. A small degradation parameter, ϕ_c, yields quasi-integral behavior. The steady-state behavior of the BC (orange/red) is less sensitive to the leak parameter when compared with the LMSC.

(F) When the output of the BC is produced and degraded (see schematic in Figure 3F), we lose the ability to track the reference. Here, $\rho_c = 0.5\delta_c$, in which case ultrasensitivity is lost as shown in Figure 3D; in this case, unlike the LMSC, the steady-state error cannot be reduced if ϕ_c is small. In general, the overshoot observed in the BC is larger than the LMSC, which may be an undesirable transient behavior. Nominal parameters used for both controllers and process are in Table 1 and are comparable to those adopted in recent computational studies of the LMSC (Table S6).

harnessed to build a BC, with RNA sequestration being easier to design because it takes advantage of well-understood Watson-Crick base pairing. These alternate BCs are used for closed-loop regulation of molecular processes with different complexity, an *in vitro* transcriptional network and *in vivo* expression of a protein of interest (transcription-translation).

RNA-based brink controllers

RNA molecules are emerging as versatile, programmable components for control of gene expression (Chappell et al., 2015; Kim and Franco, 2020). Complex RNA-based reaction networks can be realized thanks to the systematic design of multiple domains with distinct functions (Groves et al., 2016; Green et al., 2017). RNA molecules enjoy other important advantages such as a low metabolic burden (because they do not require translation), portability (synthetic RNA molecules are not host-specific), and fast response times (production and degradation rates of RNA are generally faster than proteins). We examine two potential BC implementations that take advantage of RNA molecules within *in vitro* and *in vivo* examples.

Control of a synthetic transcriptional network using an aptamer brink controller

Aptamers are RNA molecules that bind to target ligands regulating their function, and they can be artificially selected via SELEX (Stoltenburg et al., 2007). Here, we propose to build a BC using aptamers that bind to and deactivate viral RNA polymerases (RNAP) (Mori et al., 2012; Ohuchi et al., 2012). Figure 5A, right, shows that the comparator is built with two RNA species, R_I and R_A, which are, respectively, an aptamer and a complementary anti-aptamer produced with synthetic templates (A, I) as recently shown by (Lloyd et al., 2018). RNA aptamer, R_I, binds to and represses a viral RNAP, the output U of the controller. The anti-aptamer, R_A, displaces the aptamer, reactivating RNAP.

We examine the aptamer BC as a closed-loop molecular controller for an *in vitro* synthetic transcriptional circuit (genelet) (Kim et al., 2006; Franco et al., 2011; Weitz et al., 2014) shown in Figure 5A, right. Here, Y is a linear template whose promoter is partially incomplete and is activated by hybridization of a single-stranded DNA activator molecule, W. The template is deactivated by an RNA inhibitor molecule, Z, transcribed by U; Z displaces W via toehold-mediated branch migration and converts Y to inactive Y^* (Kim et al., 2006). Additionally, Z directly binds to W converting it into inactive W^*; we assume that W^* spontaneously reverts to its active form W. The control objective is to maintain a constant active genelet concentration, y, despite uncertainty in the activity of the enzymes and in the value of the reaction rate constants. The reactions and the corresponding ODE model (controller and process) are reported in Section S4.1, where we also show that the closed-loop system always presents a unique equilibrium that remains stable in a range of parameter values.

The response of the closed-loop system to changes in individual parameters is in Figure S6. Because, in practice, all parameters may vary at the same time, in Figures 5B1–5B3 we report the behavior of the system when the nominal parameters of the process are (all) randomly drawn in an interval of ±20% of their nominal value (Table S2). When comparing the steady-state behavior versus the normalized reference value $\bar{r}$, a reduced sensitivity (tighter, linear trend) of the closed-loop circuit (dark blue circles) is noted relative to the circuit operating in open-loop (light blue circles). Simultaneous variation of both the process and controller parameters shows a similar trend, albeit with a broader steady-state variability in closed loop (Figure S7). The controller handles uncertainty in the parameters more robustly when the total concentration of controller output, u^{tot}, is increased (panel B3), thereby increasing its range. In the insets, example equilibrium maps are plotted which correspond to parameter combinations that yield the desired reference tracking or fail to perform. These plots confirm that the steady-state error is small when the input-output maps intersect in the ultrasensitive region of the controller, while it increases if the intersection occurs in the saturation region.

A toehold switch brink controller for control of protein expression

Toehold switches are engineered bacterial riboregulators that take advantage of the paradigm of toehold-mediated strand displacement (Green et al., 2017). We suggest a BC implementation with toehold switches where the comparator is built with two complementary RNA species that mutually sequester each other (Figure 5C, left). Species U^* is a constitutively inactive toehold RNA switch, because a programed secondary structure prevents translation by hindering access of the ribosome to the RBS region. RNA species (R_A) is designed to bind to U^* and convert it in the active complex U, to which the ribosome can bind and start translation. In the proposed design, R_A includes a toehold that makes it possible for R_I to displace R_A from U, thereby deactivating it. We assume Hill-type induction of R_A and R_I, a short half-life of R_A and R_I (12 min), as well as the production and degradation of RNA species U (Section S4.2). Activation and deactivation rate constants of U are assumed to be as fast as RNA hybridization and toehold-mediated strand displacement *in vitro* (Table S3).

We test the ability of the toehold switch BC to control a protein expression process with output Y (17) within a negative feedback loop. To begin, we assume the total amount of U is constant. Figure 5D1 compares the closed-loop with the open-loop system in which Y is controlled with an inducer. The nominal parameters of the process were varied by randomly perturbing them in the interval of ±20% their nominal value. The closed-loop system presents a single equilibrium that was found by computing the intersection of the input-output maps of the controller and the process (Section S4.2); stability of the equilibrium was tested by checking the eigenvalues of the Jacobian matrix. Figure 5D1 shows a linear trend relating the reference and the steady-state output of the (closed-loop) process. Poor performance occurs when the equilibrium falls in the saturated region of the controller (inset plot), but the controller handles the majority of random parameter combinations well (Figure 5D2). Parametric perturbations of both the controller and the process, up to 50%, show similar trends, although with broader variability (Figure S8). The effects of changing individual parameters are shown in Figure S9, and they are generally consistent with those shown in Figure 4. Next, we modeled the production and degradation of U that is expected to occur for RNA molecules. Figure 5D3 shows that the controller performance can be compromised in the presence of the production

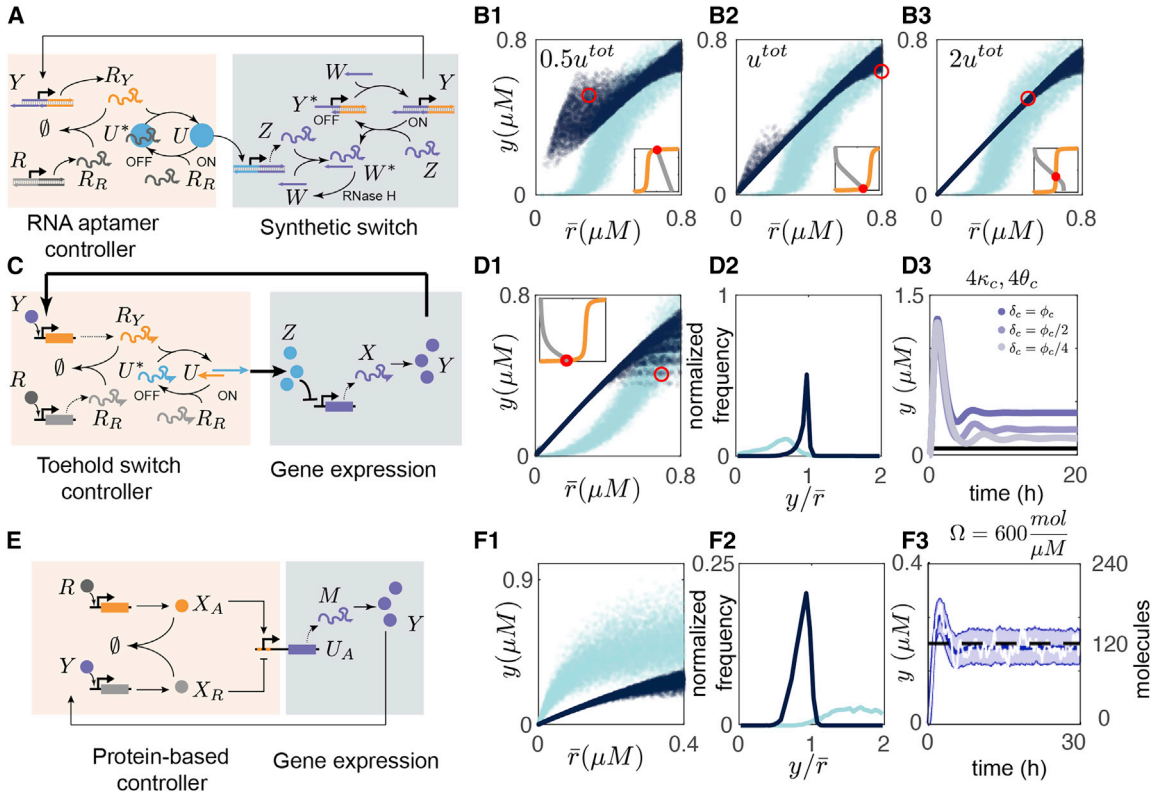

Figure 5. Computational analysis of different BC implementations to regulate target RNA or protein expression

The reactions of the BC could be realized with different components as long as it is possible to program a sequestration reaction followed by an activation/deactivation cycle. Here, we illustrate different realizations and test their performance on controlling simple gene networks *in vitro* and *in vivo* (A, C, and E). In (B1), (B2), (B3), (D1), and (F1), we illustrate the capacity of the closed-loop system to maintain reference tracking in the presence of parameter uncertainty of the process. Steady-state plots, including 10,000 equilibrium points, each computed from a random parameter draw (±20% of their nominal values). Steady states were found analytically (open loop, cyan circles), or computationally as intersections of equilibrium conditions (closed-loop, dark blue circles). Open-loop and closed-loop steady-state conditions are reported in Sections S4.1–S4.4; stability was checked by evaluating the eigenvalues of the Jacobian matrix. Additional simulations with broader random parameter perturbations for both the process and the controller are in Figures S6, S10, and S13.

(A) Schematic of the reactions for an aptamer-based BC, applied to the closed-loop control of a synthetic genelet (Kim et al., 2006).

(B1–B3) Simulations showing that the BC achieves linear reference tracking (dark blue), outperforming the open-loop system (cyan). Increasing improves the closed-loop system performance. Insets show example equilibrium maps.

(C) Schematic of a toehold switch BC controlling a protein expression process.

(D1 and D2) We compare the ability of the output of the closed-loop (dark blue) and open-loop (light blue) systems to achieve a desired protein reference level. The closed-loop system linearly tracks the reference, outperforming the open-loop system in the majority of parameter combinations (D2). All equilibria in this simulation are stable.

(D3) If component U^* is produced and degraded at rates ρ_c, δ_c ($\rho_c = 0.5\delta_c$), the controller performance degrades but can be recovered as long these rates are small while the maximal rates of production of κ_c (X_A) and θ_c (X_R) are large. The reference is shown in black.

(E) Protein heterodimer BC used for control of gene expression.

(F1 and F2) For random process parameter perturbations, the steady-state closed-loop system tracks the reference with a linear trend. In this simulation, 76% of the closed-loop equilibria plotted are stable, and 23% of the equilibria are unstable.

(F3) Example stochastic simulations show that the closed-loop system operates near the desired reference ($\Omega = N_A \cdot V$, where N_A is Avogadro's number and $V = 1$ fL). At a lower copy number, the variance increases (Figure S13); however, bimodality is not observed.

of U^* (parameter ρ_c) and degradation of both U^* and U (parameter δ_c), a result consistent Figure 4E (see also Production and degradation of the output species reduce ultrasensitivity). This issue is mitigated if δ_c is substantially slower than the controller degradation parameter ϕ_c (degradation of Y_R and R_R); $\rho_c = 0.5\delta_c$ is used to guarantee an equilibrium value $u^{tot} \approx 500nM$. Consistent with expression (Equation 11), it is helpful if the production rate constants κ_c and θ_c are larger than their nominal value.

In Section S4.3 the toehold switch BC is also examined as a closed-loop controller for biofuel production, previously considered in (Briat and Khammash, 2018) as a test case for the antithetic MSC controller. The closed-loop system generally tracks the reference; however, oscillatory instability happens in over 20% of the parameter combinations that were randomly tested. The emergence of a limit cycle was also reported in (Briat and Khammash, 2018), when the sequestration parameter of the antithetic controller is too large. This confirms a trade-off between performance and stability known for MSCs (Olsman et al., 2019). By reducing the production rate constants of R_R and R_Y the system becomes stable, at the expense of a slower temporal response (Figures S10 and S11).

A protein heterodimer brink controller

Recent advances in protein engineering have made it possible to design synthetic protein-protein and protein-DNA interactions in a modular way, opening new routes toward the construction of complex protein circuits and feedback loops (Chen et al., 2020). Here, we examine a BC implementation in which proteins are designed to interact via sequestration by forming a heterodimer. They are also designed to regulate the active or inactive state of a promoter as output of the controller, as illustrated in Figure 5E. Because the number of DNA-binding sites are tightly regulated in cells, this architecture should maintain a constant total controller output, minimizing the steady-state error caused by total output fluctuations expected with the toehold switch implementations. The model of the protein heterodimer BC is derived and analyzed in Section S4.4 and nominal parameters are in Table S5.

Unlike the ideal BC, the output state is not directly switched between the active and the inactive form, rather, this is possible because of rapid changes to the dynamic equilibrium of the free promoter. Assuming the activator and the repressor have the same promoter dissociation constant K_c, the output of the heterodimer BC (active promoter u_A) at steady state is:

$$\bar{u}_A = \left(\frac{\bar{X}_A^2}{K_c^2 + \bar{X}_A^2 + \bar{X}_R^2} \right) u^{tot}.$$

If K_c is small, this expression is comparable to the steady-state output of the ideal BC in Equation 22 (the Hill coefficient $n = 2$ is due to dimerization), but a large K_c can compromise the input-output map, introducing a bias in the feedback loop. However, ultrasensitivity of the response improves when including both an activator, X_A, and a repressor, X_R, competing to control the hybrid promoter (Figure S13). This is consistent with the analysis of the ''single rail'' BC, and Figure 3F, which shows that regulation of both activation and deactivation is essential for ultrasensitivity.

We test the ability of the protein heterodimer BC to regulate expression of a protein Y, so that it tracks a reference concentration despite uncertainty in the process reaction rates (Figure 5C). The simplest open-loop approach to achieve a desired reference concentration of Y is to titrate the concentration of its inducer Y. However, this approach yields a nonlinear reference-output map that is sensitive to perturbations in the process parameters as shown in Figure 5F1 (light blue dots), where all process parameters are allowed to vary simultaneously by ± 20% of their nominal value. The output variability is considerably reduced when the heterodimer BC is included as a closed-loop controller. Despite the process variability, the closed-loop steady-state follows the reference with a linear trend (blue dots) for the majority of random parameter combinations (Figure 5F2). Under parametric perturbations for both the controller and the process, up to 50% (Figure S16), the performance of the closed-loop system deteriorates, but a linear reference-output trend is still discernible for the closed-loop system. Illustrative stochastic simulations in Figure 5F3 show the mean and variance of an ensemble of 500 closed-loop trajectories, with one example trajectory shown in white. The mean of the trajectories is very close to the reference, consistent with the deterministic simulations shown in Figures S14 and S15. Section S3.11 reports simulation details, and additional stochastic runs at lower copy number (Figure S17).

This synthetic heterodimer controller may be experimentally realized in many ways. The most immediate implementation could take advantage of the degronLOCKR system, which was recently used to build feedback loops in (Ng et al., 2019). This pathway could be tuned to achieve input-output ultrasensitivity and minimize steady-state error. Additional routes would be to use tetR heterodimers or Lux-R sequestration (Baron et al., 1999; DeLateur, 2019). In general, a variety of heterodimers can be engineered *de novo* by integrating modular protein-protein interfaces (Chen et al., 2020) and DNA-binding domains (Schmidl et al., 2019).

DISCUSSION

Feedback controllers in synthetic biology have the potential to mitigate many challenges that limit the performance and scalability of nonlinear molecular circuits, such as uncertainty, sensitivity to disturbances, and lack of modularity (Del Vecchio et al., 2016). This document has covered how ultrasensitive components can serve as molecular controllers for closed-loop reference tracking and disturbance rejection and can guarantee robust operations despite uncertainty in the process parameters. Ultrasensitivity concerns the stationary input-output map of the controller, and we showed that if the threshold can be set by an external reference, then the unique closed-loop equilibrium of the system is naturally forced to operate near the reference in a robust manner. The BC was described as a particular reaction network yielding an ultrasensitive controller with a tunable threshold that takes advantage of molecular sequestration by directing both activation and deactivation of an output molecule. We examined its advantages, discussed its limitations, and proposed different implementation routes considering realistic simulation parameters. RNA molecules (aptamers and toehold switches) or protein heterodimers can be engineered to perform mutual sequestration and activation/deactivation of the controller output. As RNA-based synthetic biology and tools for protein engineering are rapidly expanding (Chappell et al., 2015; Lehr et al., 2019; Chen et al., 2020), the BC may be a useful architecture to build homeostatic and adaptive systems.

Ultrasensitive controllers as a high-gain feedback mechanism

Ultrasensitive components are common in nature (Zhang et al., 2013). For example, the yeast osmoregulation system combines ultrasensitivity of the MAPK pathway with negative feedback to achieve perfect adaptation (Muzzey et al., 2009). Adaptation has also been observed in ultrasensitive enzymatic networks examined using *in silico* evolutionary algorithms (Feng et al., 2016). A parallel can be drawn between ultrasensitive modules in a biological feedback loop and high-gain feedback controllers in engineering. High-gain negative feedback is known to improve the reliability of systems that are uncertain: operational amplifiers are a classical example that illustrate how the output of a high-gain device can track the input, despite uncertainty in the gain, as long as negative feedback is present. Furthermore, high-gain feedback linearizes the input-output map, a feature recently described in ultrasensitive molecular signaling pathways (Nunns

and Goentoro, 2018) and observed in our implementation examples (Figures 5B2, 5B3, 5D1, and 5F1). Potential disadvantages of high-gain controllers include instability, which may introduce oscillations (Kholodenko, 2000; Briat et al., 2016a) and chattering, a phenomenon where the controller rapidly switches between its on and off states, which often occurs in sliding mode controllers (Montefusco et al., 2016). Instability is of concern in sequestration-based controllers, like the one described here, and can be prevented by limiting the closed-loop gain, which generally depends on several parameters (Briat and Khammash, 2018; Olsman et al., 2019). If the process gain is fixed, this gain reduction will fall on the controller and possibly reduce its ultrasensitivity. This points to a general trade-off between stability and performance in most control systems. The issue of chattering is not expected to occur in our setup, because ultrasensitivity is required at steady state. Switching between the controller minimum and maximum output is not observed in the computational analysis, including stochastic simulations in Section 3.11, even though the controller converges to steady state faster than the process in the examples.

Performance trade-offs and tuning of molecular controllers

An important aspect of this analysis is that it distinguishes the roles of gain and setpoint in a molecular controller, which may be tuned in isolation prior to closed-loop implementation. This strategy may enable the development of ''universal'' RNA or protein controllers that may be swapped to regulate a variety of processes with focused adjustments in threshold and gain, similar to PID controllers in industrial settings (Lehr et al., 2019; Langan et al., 2019). Ultrasensitive controllers could be built with a variety of strategies (Box 1), but it may be challenging to independently tune the gain (steepness of the response) and threshold. We showed that this is possible by combining sequestration reactions (comparator) (Agrawal et al., 2015; Scalise and Schulman, 2016) and an activation/deactivation cycle (switch) (Cuba Samaniego and Franco, 2017a, 2017b), which constitute the BC. The threshold is determined primarily by the concentration of the fixed input of the comparator, which therefore operates as a reference signal. In contrast, the slope of the ultrasensitive response, which is considered the gain of the controller, is determined by multiple reaction rate constants and is drastically improved by including both activation and deactivation. Overall, the ultrasensitive gain of the BC can be increased through multiple tuning knobs and it results from the interconnection of components that do not have to be ultrasensitive in isolation; this may be an advantage over simpler architectures where it may be more challenging to increase the gain with fewer parameters. According to our computational analysis, the BC is ultrasensitive when adopting sequestration and switching rate constants that are realistic for RNA and protein components (Figure 3; Tables 1 and S6). Yet, we have shown an important limitation of the BC: its performance becomes worse if its output is produced and degraded, and its total mass is not conserved. This limitation may be mitigated in practice if the output of the BC is a DNA-binding site or another species whose level is tightly regulated, naturally. Ultrasensitive controllers that are radically different from the BC may not suffer from this limitation. We have also discussed how an output load reduces the range of ultrasensitive operation of the BC, as the fraction of available output is depleted, yet it does not compromise ultrasensitivity per se.

Molecular sequestration is important to achieve integral feedback

Many molecular networks for closed-loop control rely exclusively on molecular sequestration (Franco et al., 2014; Hsiao et al., 2015; Annunziata et al., 2017; Kelly et al., 2018; Huang et al., 2018; Aoki et al., 2019), which is sufficient to achieve homeostasis under conditions such as absence of degradation or very fast controller dynamics (Briat et al., 2016a; Huang et al., 2018; Qian and Del Vecchio, 2018) (Table S6). Our analysis is consistent with these results, because sequestration alone is known to yield an ultrasensitive response with a tunable threshold and a large gain, in particular when degradation is negligible and sequestration is fast (Buchler and Cross, 2009; Mukherji et al., 2011). Sequestration also provides fast kinetic responses in natural pathways (Shimoni et al., 2007). Because the speed of a feedback controller is critical for performance, ultrasensitive controllers that include sequestration would take advantage of its speed, simplicity, and tunability. Although this research has focused on steady-state properties of the BC, we found that its convergence is comparable with that of other sequestration-based controllers, and that the activation/deactivation cycle improves the controller gain without compromising speed. However, it is important to note that while multi-stage cascades may sharpen an ultrasensitive response (Huang and Ferrell, 1996), they can also introduce delays and promote the emergence of oscillations (Kholodenko, 2000).

Conclusions and outlook

We have discussed the idea that ultrasensitive components can enable quasi-integral control within molecular feedback circuits. In the context of ''reverse engineering'' biological networks, this analysis supports the view that ultrasensitivity may be a key property for adaptation (Muzzey et al., 2009). Yet, ultrasensitive modules may not be immediately recognized because a sharp response can arise from the composition of diverse processes (Zhang et al., 2013). In the context of ''forward engineering'' biological controllers, we contribute a relatively simple design principle to build robust feedback loops, since ultrasensitivity may be achieved by a variety of mechanisms (Box 1) (Zhang et al., 2013). The design of such mechanisms must takes into account their speed of convergence and the possibility of closed-loop instability (Olsman et al., 2019). Sequestration is a viable approach to obtain a tunable ultrasensitive response, which is enhanced by the combination with an activation/deactivation cycle. This suggests that it may be beneficial to combine multiple layers of regulation to obtain ultrasensitive controllers. Furthermore, multiple controllers may be combined in parallel to implement a dual rail actuator with opposite effects (activation and repression) on the process (Cuba Samaniego and Franco, 2017b; Gupta and Khammash, 2019; Cuba Samaniego et al., 2019). Recent advances in RNA design and protein engineering provide many routes toward the synthesis of regulators with a tunable threshold and gain (Lee et al., 2018; Kim et al., 2019; Chen et al., 2020). Their application as molecular feedback controllers may be guided by the mathematical models, design principles, and trade-offs we illustrated.

STAR★METHODS

Detailed methods are provided in the online version of this paper and include the following:

- RESOURCE AVAILABILITY
  - Lead contact
  - Materials availability
  - Data and code availability
- METHODS
  - Assessing stability of closed-loop molecular networks
  - Controller requirements for *quasi*-integral behavior
  - An ultrasensitive controller operates correctly in its non-saturated regime
  - Sequestration enables error computation in the Brink Controller, and activation/deactivation increase the gain

SUPPLEMENTAL INFORMATION

Supplemental Information can be found online at https://doi.org/10.1016/j.cels.2021.01.001.

ACKNOWLEDGMENTS

We thank Yili Qian, Zoltan Tuza, Noah Olsman, Harrison Steel, Dominic Scalise, Corentin Briat, Franco Blanchini, Giulia Giordano, and Mustafa Khammash for useful comments and discussions.

This work was partially supported by the National Science Foundation through grants CMMI-1266402 and BBSRC-NSF/BIO-2020039; by the Defense Advanced Research Projects Agency through contract HR0011-16-C-01-34; and by the US Department of Energy, Office of Science, Office of Basic Energy Sciences, under award number DESC0010595, which partially supported salary to E.F. and to C.C.S.

AUTHOR CONTRIBUTIONS

C.C.S. and E.F. conceived and designed research, developed the models, and conducted mathematical analysis. C.C.S. performed computational simulations. Both authors wrote the paper.

DECLARATION OF INTERESTS

The authors declare no competing interests.

Received: March 18, 2019
Revised: September 22, 2020
Accepted: January 11, 2021
Published: February 3, 2021

SUPPORTING CITATIONS

The following references appear in the Supplemental information: Basu et al. (2005); Blanchini and Franco (2011); Blanchini and Miani (2008); Dunlop et al. (2010); Enciso (2005); Gillespie (1977); Kamar et al. (2017); Liu et al. (2003); Milo et al. (2010); Normanno et al. (2015); Qian et al. (2017); Richeson and Wiseman (2002); Sontag (2005).

REFERENCES

Agrawal, D.K., Franco, E., and Schulman, R. (2015). A self-regulating biomolecular comparator for processing oscillatory signals. J. R. Soc. Interface *12*, 20150586.

Agrawal, D.K., Marshall, R., Noireaux, V., and Sontag, E.D. (2019). In vitro implementation of robust gene regulation in a synthetic biomolecular integral controller. Nat. Commun. *10*, 5760.

Agrawal, D.K., Tang, X., Westbrook, A., Marshall, R., Maxwell, C.S., Lucks, J., Noireaux, V., Beisel, C.L., Dunlop, M.J., and Franco, E. (2018). Mathematical modeling of RNA-based architectures for closed loop control of gene expression. ACS Synth. Biol. *7*, 1219–1228.

Ang, J., Bagh, S., Ingalls, B.P., and McMillen, D.R. (2010). Considerations for using integral feedback control to construct a perfectly adapting synthetic gene network. J. Theor. Biol. *266*, 723–738.

Angeli, D., and Sontag, E.D. (2003). Monotone control systems. IEEE Trans. Automat. Contr. *48*, 1684–1698.

Annunziata, F., Matyjaszkiewicz, A., Fiore, G., Grierson, C.S., Marucci, L., di Bernardo, M., and Savery, N.J. (2017). An orthogonal multi-input integration system to control gene expression in Escherichia coli. ACS Synth. Biol. *6*, 1816–1824.

Aoki, S.K., Lillacci, G., Gupta, A., Baumschlager, A., Schweingruber, D., and Khammash, M. (2019). A universal biomolecular integral feedback controller for robust perfect adaptation. Nature *570*, 533–537.

Åström, K.J., and Murray, R.M. (2010). Feedback Systems: An Introduction for Scientists and Engineers (Princeton University Press).

Baron, U., Schnappinger, D., Helbl, V., Gossen, M., Hillen, W., and Bujard, H. (1999). Generation of conditional mutants in higher eukaryotes by switching between the expression of two genes. Proc. Natl. Acad. Sci. USA *96*, 1013–1018.

Basu, S., Gerchman, Y., Collins, C.H., Arnold, F.H., and Weiss, R. (2005). A synthetic multicellular system for programmed pattern formation. Nature *434*, 1130–1134.

Blanchini, F., and Franco, E. (2011). Structurally robust biological networks. BMC Syst. Biol. *5*, 74.

Blanchini, F., and Miani, S. (2008). Set-Theoretic Methods in Control (Springer).

Bloom, R.J., Winkler, S.M., and Smolke, C.D. (2015). Synthetic feedback control using an RNAi-based gene-regulatory device. J. Biol. Eng. *9*, 5.

Bonnet, J., Subsoontorn, P., and Endy, D. (2012). Rewritable digital data storage in live cells via engineered control of recombination directionality. Proc. Natl. Acad. Sci. USA *109*, 8884–8889.

Briat, C., Gupta, A., and Khammash, M. (2016a). Antithetic integral feedback ensures robust perfect adaptation in noisy biomolecular networks. Cell Syst *2*, 15–26.

Briat, C., and Khammash, M. (2018). Perfect adaptation and optimal equilibrium productivity in a simple microbial biofuel metabolic pathway using dynamic integral control. ACS Synth. Biol. *7*, 419–431.

Briat, C., Zechner, C., and Khammash, M. (2016b). Design of a synthetic integral feedback circuit: dynamic analysis and DNA implementation. ACS Synth. Biol. *5*, 1108–1116.

Buchler, N.E., and Cross, F.R. (2009). Protein sequestration generates a flexible ultrasensitive response in a genetic network. Mol. Syst. Biol. *5*, 272.

Buchler, N.E., and Louis, M. (2008). Molecular titration and ultrasensitivity in regulatory networks. J. Mol. Biol. *384*, 1106–1119.

Chappell, J., Watters, K.E., Takahashi, M.K., and Lucks, J.B. (2015). A renaissance in RNA synthetic biology: new mechanisms, applications and tools for the future. Curr. Opin. Chem. Biol. *28*, 47–56.

Chen, H., Shiroguchi, K., Ge, H., and Xie, X.S. (2015). Genome-wide study of mRNA degradation and transcript elongation in Escherichia coli. Mol. Syst. Biol. *11*, 781.

Chen, Z., Kibler, R.D., Hunt, A., Busch, F., Pearl, J., Jia, M., VanAernum, Z.L., Wicky, B.I.M., Dods, G., Liao, H., et al. (2020). De novo design of protein logic gates. Science *368*, 78–84.

Cuba Samaniego, C., Delateur, N.A., Giordano, G., and Franco, E. (2019). Biomolecular stabilisation near the unstable equilibrium of a biological system. IEEE 58th Conference on Decision and Control (CDC), 958–964.

Cuba Samaniego, C., and Franco, E. (2017a). An ultrasensitive biomolecular network for robust feedback control. IFAC-PapersOnLine *50*, 10950–10956.

Cuba Samaniego, C., and Franco, E. (2017b). An ultrasensitive motif for robust closed loop control of biomolecular systems. In Decision and Control (CDC), 2017 IEEE 56th Annual Conference, pp. 5334–5340.

Cuba Samaniego, C., and Franco, E. (2018). A robust molecular network motif for period-doubling devices. ACS Synth. Biol. *7*, 75–85.

Cuba Samaniego, C., Giordano, G., Kim, J., Blanchini, F., and Franco, E. (2016). Molecular titration promotes oscillations and bistability in minimal network models with monomeric regulators. ACS Synth. Biol. *5*, 321–333.

Darzacq, X., Shav-Tal, Y., De Turris, V., Brody, Y., Shenoy, S.M., Phair, R.D., and Singer, R.H. (2007). In vivo dynamics of RNA polymerase II transcription. Nat. Struct. Mol. Biol. *14*, 796–806.

De Palo, G., Facchetti, G., Mazzolini, M., Menini, A., Torre, V., and Altafini, C. (2013). Common dynamical features of sensory adaptation in photoreceptors and olfactory sensory neurons. Sci. Rep. *3*, 1251.

Del Vecchio, D., Dy, A.J., and Qian, Y. (2016). Control theory meets synthetic biology. J. R. Soc. Interface *13*, 20160380.

Del Vecchio, D., and Murray, R.M. (2015). Biomolecular Feedback Systems (Princeton University Press).

Del Vecchio, D., Ninfa, A.J., and Sontag, E.D. (2008). Modular cell biology: retroactivity and insulation. Mol. Syst. Biol. *4*, 161.

DeLateur, N.A. (2019). Engineering LuxR-type quorum sensing proteins for new functions, Ph.D. Thesis (Department of Chemistry, Massachusetts Institute of Technology).

Doyle, J.C., Francis, B.A., and Tannenbaum, A. (1992). Feedback Control Theory, *Vol. 134* (MacMillan).

Dunlop, M.J., Keasling, J.D., and Mukhopadhyay, A. (2010). A model for improving microbial biofuel production using a synthetic feedback loop. Syst. Synth. Biol. *4*, 95–104.

Enciso, G.A. (2005). Monotone input/output systems, and applications to biological systems, Ph.D. Thesis (Rutgers, the State University of New Jersey).

Feng, S., Ollivier, J.F., and Soyer, O.S. (2016). Enzyme sequestration as a tuning point in controlling response dynamics of signalling networks. PLoS Comp. Biol. *12*, e1004918.

Ferrell, J.E. (2009). Q&A: cooperativity. J. Biol. *8*, 53.

Ferrell, J.E., and Ha, S.H. (2014). Ultrasensitivity part i: michaelian responses and zero-order ultrasensitivity. Trends Biochem. Sci. *39*, 496–503.

Folliard, T., Steel, H., Prescott, T.P., Wadhams, G., Rothschild, L.J., and Papachristodoulou, A. (2017). A synthetic recombinase-based feedback loop results in robust expression. ACS Synth. Biol. *6*, 1663–1671.

Franco, E., Friedrichs, E., Kim, J., Jungmann, R., Murray, R., Winfree, E., and Simmel, F.C. (2011). Timing molecular motion and production with a synthetic transcriptional clock. Proc. Natl. Acad. Sci. USA *108*, E784–E793.

Franco, E., Giordano, G., Forsberg, P.O., and Murray, R.M. (2014). Negative autoregulation matches production and demand in synthetic transcriptional networks. ACS Synth. Biol. *3*, 589–599.

Gillespie, D.T. (1977). Exact stochastic simulation of coupled chemical reactions. J. Phys. Chem. *81*, 2340–2361.

Goldbeter, A., and Koshland, D.E. (1981). An amplified sensitivity arising from covalent modification in biological systems. Proc. Natl. Acad. Sci. USA *78*, 6840–6844.

Golding, I., Paulsson, J., Zawilski, S.M., and Cox, E.C. (2005). Real-time kinetics of gene activity in individual bacteria. Cell *123*, 1025–1036.

Green, A.A., Kim, J., Ma, D., Silver, P.A., Collins, J.J., and Yin, P. (2017). Complex cellular logic computation using ribocomputing devices. Nature *548*, 117–121.

Groves, B., Chen, Y.J., Zurla, C., Pochekailov, S., Kirschman, J.L., Santangelo, P.J., and Seelig, G. (2016). Computing in mammalian cells with nucleic acid strand exchange. Nat. Nanotechnol. *11*, 287–294.

Gupta, A. and Khammash, M. (2019). An antithetic integral rein controller for bio-molecular networks. IEEE 58th Conference on Decision and Control (CDC), pp. 2808–2813.

Hooshangi, S., Thiberge, S., and Weiss, R. (2005). Ultrasensitivity and noise propagation in a synthetic transcriptional cascade. Proc. Natl. Acad. Sci. USA *102*, 3581–3586.

Hsiao, V., de los Santos, E.L., Whitaker, W.R., Dueber, J.E., and Murray, R.M. (2015). Design and implementation of a biomolecular concentration tracker. ACS Synth. Biol. *4*, 150–161.

Huang, C.Y., and Ferrell, J.E. (1996). Ultrasensitivity in the mitogen-activated protein kinase cascade. Proc. Natl. Acad. Sci. USA *93*, 10078–10083.

Huang, H.H., Qian, Y., and Del Vecchio, D. (2018). A quasi-integral controller for adaptation of genetic modules to variable ribosome demand. Nat. Commun. *9*, 5415.

Kajita, M.K., Aihara, K., and Kobayashi, T.J. (2017). Balancing specificity, sensitivity, and speed of ligand discrimination by zero-order ultraspecificity. Phys. Rev. E *96*, 012405.

Kamar, R.I., Banigan, E.J., Erbas, A., Giuntoli, R.D., Olvera de la Cruz, M.O., Johnson, R.C., and Marko, J.F. (2017). Facilitated dissociation of transcription factors from single DNA binding sites. Proc. Natl. Acad. Sci. USA *114*, E3251–E3257.

Kelly, C.L., Harris, A.W.K., Steel, H., Hancock, E.J., Heap, J.T., and Papachristodoulou, A. (2018). Synthetic negative feedback circuits using engineered small RNAs. Nucleic Acids Res *46*, 9875–9889.

Kemmer, C., Gitzinger, M., Daoud-El Baba, M., Djonov, V., Stelling, J., and Fussenegger, M. (2010). Self-sufficient control of urate homeostasis in mice by a synthetic circuit. Nat. Biotechnol. *28*, 355–360.

Khalil, H.K. (1996). Nonlinear Systems (Prentice-Hall).

Kholodenko, B.N. (2000). Negative feedback and ultrasensitivity can bring about oscillations in the mitogen-activated protein kinase cascades. Eur. J. Biochem. *267*, 1583–1588.

Kim, J., Khetarpal, I., Sen, S., and Murray, R.M. (2014). Synthetic circuit for exact adaptation and fold-change detection. Nucleic Acids Res *42*, 6078–6089.

Kim, J., and Franco, E. (2020). RNA nanotechnology in synthetic biology. Curr. Opin. Biotechnol. *63*, 135–141.

Kim, J., White, K.S., and Winfree, E. (2006). Construction of an *in vitro* bistable circuit from synthetic transcriptional switches. Mol. Syst. Biol. *2*, 68.

Kim, J., Zhou, Y., Carlson, P.D., Teichmann, M., Chaudhary, S., Simmel, F.C., Silver, P.A., Collins, J.J., Lucks, J.B., Yin, P., and Green, A.A. (2019). De novo-designed translation-repressing riboregulators for multi-input cellular logic. Nat. Chem. Biol. *15*, 1173–1182.

Langan, R.A., Boyken, S.E., Ng, A.H., Samson, J.A., Dods, G., Westbrook, A.M., Nguyen, T.H., Lajoie, M.J., Chen, Z., Berger, S., et al. (2019). De novo design of bioactive protein switches. Nature *572*, 205–210.

Lee, Y.J., Kim, S.J., and Moon, T.S. (2018). Multilevel regulation of bacterial gene expression with the combined STAR and antisense RNA system. ACS Synth. Biol. *7*, 853–865.

Lehr, F.X., Hanst, M., Vogel, M., Kremer, J., Göringer, H.U., Suess, B., and Koeppl, H. (2019). Cell-free prototyping of AND-logic gates based on heterogeneous RNA activators. ACS Synth. Biol. *8*, 2163–2173.

Lillacci, G., Benenson, Y., and Khammash, M. (2018). Synthetic control systems for high performance gene expression in mammalian cells. Nucleic Acids Res *46*, 9855–9863.

Liu, M., Gupte, G., Roy, S., Bandwar, R.P., Patel, S.S., and Garges, S. (2003). Kinetics of transcription initiation at lacP1. Multiple roles of cyclic AMP receptor protein. J. Biol. Chem. *278*, 39755–39761.

Lloyd, J., Tran, C.H., Wadhwani, K., Cuba Samaniego, C., Subramanian, H.K.K., and Franco, E. (2018). Dynamic control of aptamer–ligand activity using strand displacement reactions. ACS Synth. Biol. *7*, 30–37.

Milo, R., Jorgensen, P., Moran, U., Weber, G., and Springer, M. (2010). BioNumbers - the database of key numbers in molecular and cell biology. Nucleic Acids Res *38*, D750–D753.

Milo, R., and Phillips, R. (2015). Cell Biology by the Numbers (Garland Science).

Montefusco, F., Akman, O.E., Soyer, O.S., and Bates, D.G. (2016). Ultrasensitive negative feedback control: a natural approach for the design of synthetic controllers. PLoS One *11*, e0161605.

Mori, Y., Nakamura, Y., and Ohuchi, S. (2012). Inhibitory RNA aptamer against SP6 RNA polymerase. Biochem. Biophys. Res. Commun. *420*, 440–443.

Mukherji, S., Ebert, M.S., Zheng, G.X., Tsang, J.S., Sharp, P.A., and van Oudenaarden, A. (2011). MicroRNAs can generate thresholds in target gene expression. Nat. Genet. *43*, 854–859.

Muzzey, D., Gómez-Uribe, C.A., Mettetal, J.T., and van Oudenaarden, A. (2009). A systems-level analysis of perfect adaptation in yeast osmoregulation. Cell *138*, 160–171.

Nevozhay, D., Adams, R.M., Murphy, K.F., Josic, K., and Balázsi, G. (2009). Negative autoregulation linearizes the dose–response and suppresses the heterogeneity of gene expression. Proc. Natl. Acad. Sci. USA *106*, 5123–5128.

Ng, A.H., Nguyen, T.H., Gómez-Schiavon, M., Dods, G., Langan, R.A., Boyken, S.E., Samson, J.A., Waldburger, L.M., Dueber, J.E., Baker, D., and El-Samad, H. (2019). Modular and tunable biological feedback control using a de novo protein switch. Nature *572*, 265–269.

Normanno, D., Boudarène, L., Dugast-Darzacq, C., Chen, J., Richter, C., Proux, F., Bénichou, O., Voituriez, R., Darzacq, X., and Dahan, M. (2015). Probing the target search of DNA-binding proteins in mammalian cells using TetR as model searcher. Nat. Commun. *6*, 7357.

Nunns, H., and Goentoro, L. (2018). Signaling pathways as linear transmitters. eLife *7*, e33617.

Ohuchi, S., Mori, Y., and Nakamura, Y. (2012). Evolution of an inhibitory RNA aptamer against T7 RNA polymerase. FEBS Open Bio *2*, 203–207.

Olsman, N., Baetica, A.A., Xiao, F., Leong, Y.P., Murray, R.M., and Doyle, J.C. (2019). Hard limits and performance tradeoffs in a class of antithetic integral feedback networks. Cell Syst *9*, 49–63.e16.

Qian, Y., and Del Vecchio, D. (2018). Realizing "integral control" in living cells: how to overcome leaky integration due to dilution? J. R. Soc. Interface *15*, 20170902.

Qian, Y., Huang, H.H., Jiménez, J.I., and Del Vecchio, D. (2017). Resource competition shapes the response of genetic circuits. ACS Synth. Biol. *6*, 1263–1272.

Ricci, F., Vallée-Bélisle, A., and Plaxco, K.W. (2011). High-precision, in vitro validation of the sequestration mechanism for generating ultrasensitive dose-response curves in regulatory networks. PLoS Comp. Biol. *7*, e1002171.

Richeson, D., and Wiseman, J. (2002). A fixed point theorem for bounded dynamical systems. Illinois J. Math. *46*, 491–495.

Scalise, D., and Schulman, R. (2016). Emulating cellular automata in chemical reaction–diffusion networks. Nat. Comput. *15*, 197–214.

Schmidl, S.R., Ekness, F., Sofjan, K., Daeffler, K.N., Brink, K.R., Landry, B.P., Gerhardt, K.P., Dyulgyarov, N., Sheth, R.U., and Tabor, J.J. (2019). Rewiring bacterial two-component systems by modular DNA-binding domain swapping. Nat. Chem. Biol. *15*, 690–698.

Shannon, B., Zamora-Chimal, C.G., Postiglione, L., Salzano, D., Grierson, C.S., Marucci, L., Savery, N.J., and Di Bernardo, M. (2020). In vivo feedback control of an antithetic molecular-titration motif in Escherichia coli using microfluidics. ACS Synth. Biol. *9*, 2617–2624.

Shimoni, Y., Friedlander, G., Hetzroni, G., Niv, G., Altuvia, S., Biham, O., and Margalit, H. (2007). Regulation of gene expression by small non-coding RNAs: a quantitative view. Mol. Syst. Biol. *3*, 138.

Shopera, T., He, L., Oyetunde, T., Tang, Y.J., and Moon, T.S. (2017). Decoupling resource-coupled gene expression in living cells. ACS Synth. Biol. *6*, 1596–1604.

Siegal-Gaskins, D., Franco, E., Zhou, T., and Murray, R.M. (2015). An analytical approach to bistable biological circuit discrimination using real algebraic geometry. J. R. Soc. Interface *12*, 20150288.

Siu, Y., Fenno, J., Lindle, J.M., and Dunlop, M.J. (2018). Design and selection of a synthetic feedback loop for optimizing biofuel tolerance. ACS Synth. Biol. *7*, 16–23.

Siuti, P., Yazbek, J., and Lu, T.K. (2013). Synthetic circuits integrating logic and memory in living cells. Nat. Biotechnol. *31*, 448–452.

Sontag, E.D. (2005). Molecular systems biology and control. Eur. J. Control *11*, 396–435.

Stoltenburg, R., Reinemann, C., and Strehlitz, B. (2007). SELEX–a (r)evolutionary method to generate high-affinity nucleic acid ligands. Biomol. Eng. *24*, 381–403.

Weitz, M., Kim, J., Kapsner, K., Winfree, E., Franco, E., and Simmel, F.C. (2014). Diversity in the dynamical behaviour of a compartmentalized programmable biochemical oscillator. Nat. Chem. *6*, 295–302.

Yi, T.M., Huang, Y., Simon, M.I., and Doyle, J. (2000). Robust perfect adaptation in bacterial chemotaxis through integral feedback control. Proc. Natl. Acad. Sci. USA *97*, 4649–4653.

You, L., Cox, R.S., Weiss, R., and Arnold, F.H. (2004). Programmed population control by cell–cell communication and regulated killing. Nature *428*, 868–871.

Zhang, D.Y., Turberfield, A.J., Yurke, B., and Winfree, E. (2007). Engineering entropy-driven reactions and networks catalyzed by DNA. Science *318*, 1121–1125.

Zhang, Q., Bhattacharya, S., and Andersen, M.E. (2013). Ultrasensitive response motifs: basic amplifiers in molecular signalling networks. Open Biol *3*, 130031.

STAR★METHODS

RESOURCE AVAILABILITY

Lead contact

Further information and requests for resources and reagents should be directed to and will be fulfilled by the Lead Contact, Elisa Franco (efranco@seas.ucla.edu).

Materials availability

This study did not generate new materials.

Data and code availability

1. This paper includes data that are generated exclusively via computational models that are deposited at https://github.com/ccubasam-code/UltrasensitiveControllers.
2. The original code is publicly available at https://github.com/ccubasam-code/UltrasensitiveControllers.
3. The scripts used to generate the figures reported in this paper are available at https://github.com/ccubasam-code/UltrasensitiveControllers.
4. Any additional information required to reproduce this work is available from the Lead Contact, Elisa Franco (efranco@seas.ucla.edu)

METHODS

Assessing stability of closed-loop molecular networks

Throughout this paper we consider a simplified context in which the process is modeled as a single-input, single-output system interconnected to a controller within a feedback loop, like the architecture in Figure 2A:

$$P:\begin{cases}\dot{x}(t)=f(x(t),u(t),p),\\ y(t)=h(x(t)),\end{cases}\qquad C:\begin{cases}\dot{z}(t)=g(z(t),y(t),q,r),\\ u(t)=w(z(t)).\end{cases}\qquad \text{(Equation 18)}$$

x and z are concentration vectors, and y and u are the concentrations of species that interconnect process and controller. The parameters characterizing each system are denoted as vectors p and q and r is a scalar reference (external input to the controller). It is assumed that both the process and the controller in isolation have a unique (non-negative), stable steady-state, which can be found by solving equations $f(x,u,p)=0$ and $g(z,y,q,r)=0$ (for fixed values of parameters and inputs). By solving equations $f(x,u,p)=0$ and $g(z,y,q,r)=0$, together with the state-to-output relations $y(t)=h(x(t))$ and $u(t)=w(z(t))$, the steady-state input-output maps k_y and k_u of each subsystem can be implicitly defined:

$$\bar{y}=k_y(u,p),\bar{u}=k_u(y,q,r). \qquad \text{(Equation 19)}$$

The steady-state values $\bar{y}$ and $\bar{u}$ of the closed-loop, interconnected system are determined by the intersections of these two maps. Having a unique equilibrium is beneficial in a closed-loop system (since the presence of multiple equilibria would make it more challenging to reach the desired one). A convenient route to ensure the existence of a unique equilibrium is to work with monotonic input-output maps, with one map that must be increasing, and the other that must be decreasing (Figure 2B). In other words, we require that $\frac{\partial}{\partial y}k_u(y,q,r)$ and $\frac{\partial}{\partial u}k_y(u,p)$ have opposite signs (for example, $\frac{\partial}{\partial y}k_u(y,q,r)>0$ and $\frac{\partial}{\partial u}k_y(u,p)<0$). This also guarantees that the overall feedback loop is negative. (Monotonicity is, however, not a necessary condition for a single closed-loop equilibrium.)

Given a unique equilibrium, there are many ways to identify its stability (stability of the process and controller in isolation does not imply that the closed-loop system is stable as well). The most direct approach is to linearize the closed-loop system, Equation 18, and examine the eigenvalues of its Jacobian matrix evaluated at the equilibrium point (Khalil, 1996). Because many biological models are monotone systems in a broad range of operating conditions, this means that the stability of a controller and process may be structurally evaluated by inspecting their Jacobian matrix (Angeli and Sontag, 2003). Analytical conditions for stability may be found in models with few variables, but this approach is impractical for realistic, large systems, whose stability must be assessed computationally.

The assumptions and the approach described here apply to all the examples we report. First, we assess stability of individual components, we then test uniqueness of the closed-loop equilibrium, and evaluate its stability through linearization and computational analysis. When possible, we provide bounds on relevant parameters to ensure stability. Each example is examined in detail in the Supplemental information file.

Controller requirements for *quasi*-integral behavior

The equilibrium of the closed-loop system is determined by the intersection of the input-output static maps shown in Figure 2B and defined by Equation 19. Perturbations of the process parameters (vector q) may cause a shift in the input-output map (gray area in

Figure 2B). However, as long as the maps are monotonic, their intersection is still unique and falls near the controller threshold $\bar{y} \approx r$ on the horizontal axis, while $\bar{u}$ takes any value inside the physically acceptable range of the controller. Therefore, if the controller input-output static map is ultrasensitive like in Figure 2B, the process steady-state may be written as:

$$\bar{y} = r + \Delta. \qquad \text{(Equation 20)}$$

This expression highlights that the difference between the steady-state output y and the reference r depends on the steepness of the off-on transition of the controller (*i.e.* its ultrasensitivity). This can be quantified with the "error" term Δ: in the limit of $\Delta \to 0$ one would achieve perfect integral control. If the controller is operating in the ultrasensitive region, Δ is bounded by the width of the transition region of the controller, $\Delta \leq \frac{1}{2}\Delta_{max}(u,q)$ (shaded yellow area in Figure 2B). It is reasonable to expect that Δ depends largely on the parameters of the controller q, rather than the parameters of the process, due to the shape of the ultrasensitive steady-state map of the controller, which forces the equilibrium point to be in a neighborhood of the reference value. By computing $\Delta_{max}(u,q)$ it is possible to find lower and upper bounds to the steady-state error, $\bar{e} = |r - \bar{y}| \leq \frac{1}{2}\Delta_{max}(u,q)$. $\Delta_{max}(u,q)$ can be found by evaluating $\bar{y} = k_y(u,p)$ at some chosen saturation values u_L and u_H of the controller, $\Delta_{max}(u,q) = k_y(u_H,p) - k_y(u_L,p)$ (Section S3.5). The width of the transition region is generally inversely proportional to the steepness, or gain, of the controller map.

An ultrasensitive controller operates correctly in its non-saturated regime

We just described how an ultrasensitive molecular controller can help track a reference (which determines the controller threshold) and reject perturbations. However, correct operation is guaranteed only if the concentration of controller species, u, does not saturate (Ang et al., 2010). If the process map intersects the controller map near saturation, it is not possible for the controller to adjust u as required to maintain the reference equilibrium. In this case, the process is not ''controllable''(this is a slight abuse of the traditional meaning of the word ''controllability'' in control theory). If the controller input-output map $k_u(\bar{y},q,r)$ is known, we can formulate a criterion to identify the range of process equilibria $\bar{y}$ that are controllable:

$$u_L + \varepsilon < k_u(\bar{y},q,r) < u_H - \varepsilon,$$

where u_L and u_H are thresholds for the controller and ε is a user-defined "safety distance" from the thresholds. These thresholds should be selected as a performance specification: if $u \leq u_L$, and $u \geq u_H$, the controller operates too close to saturation and the error term Δ in Equation 20 is too large. Given an input-output map, $k_u(\bar{y},q,r)$, in polynomial form, these inequalities can be used to find bounds on the reaction rate constants that will satisfy the specifications, and to find whether the specifications are realistic in practice for the chosen implementation of the controller. The inequalities can be examined analytically using methods such as the Routh-Hurwitz or Sturm's Theorem (Siegal-Gaskins et al., 2015; Cuba Samaniego and Franco, 2018) for simple controller networks, or characterized computationally for more complex controllers.

Sequestration enables error computation in the Brink Controller, and activation/deactivation increase the gain

The first stage of the BC includes a molecular sequestration reaction (Box 1). Taken in isolation, this reaction operates as a comparator, and at steady-state it computes the difference between its inputs. We consider the case in which input concentration a may vary, while input i is held constant. It should be noted that the same reasoning can be followed for a case in which i varies and a is constant. At steady-state, given a constant inhibitor concentration i and a fast sequestration rate, the output of the comparator can be approximated as:

$$\bar{r}_A \approx \begin{cases} 0 & a \leq k_a(i) \\ \frac{\kappa_c}{\phi_c}(a - k_a(i)) & k_a(i) \leq a \end{cases} \text{ and } \bar{r}_I \approx \begin{cases} \frac{\kappa_c}{\phi_c}(k_a(i) - a) & a \leq k_a(i) \\ 0 & k_a(i) \leq a \end{cases}, \qquad \text{(Equation 21)}$$

with a threshold $k_a(i) = \frac{\theta_c}{\kappa_c} i$. The complete derivations are in Section S2. The threshold is proportional to the input i, and therefore the threshold is tunable by setting the concentration of the inhibitor. The factor $\frac{\kappa_c}{\phi_c}$ is a steady-state gain of the reaction (*cf.* Box 1). For special cases where $\theta_c = \kappa_c$, the threshold is equal to the fixed input i. This input-output map is plotted in Figure 3B, left panel.

When a is larger than the threshold $k_a(i)$, the steady-state output of the comparator $\bar{r}_A$ is proportional to $a - k_a(i)$, which can be interpreted as the error between input a and the scaled input i with a gain $\frac{\kappa_c}{\phi_c}$. When a is smaller than the threshold, the steady-state output $\bar{r}_A$ is approximately zero. In contrast, the steady-state value of $\bar{r}_I$ is proportional to $k_a(i) - a$ when a is smaller than the threshold, and it is almost zero when a is larger than the threshold. The role of the sequestration reaction is to process the inputs by producing a distinct positive output in response to "positive" or "negative" error, thus behaving like a diode in electronic circuits. The error is computed in relation to the threshold $k_a(i)$ and the output $\bar{r}_I$ is almost zero when $\bar{r}_A$ is being produced, while output $\bar{r}_A$ is almost zero when $\bar{r}_I$ is being produced. This operation is comparable to "dual rail" logic in electronics, and an example simulation is in

Figure 3B, left panel. By examining the system's frequency response, we also show that the comparator works well on time-varying inputs $a(t)$ and $i(t)$, as long as they evolve on a timescale slower than the degradation rate constant ϕ_c (Section S2).

We now consider the activation/deactivation cycle in isolation. It receives inputs r_A and r_I, and produces the output u for the BC. The equilibrium value $\overline{u}$, for constant inputs r_A and r_I, is given by the following Michaelian function:

$$\overline{u} = \frac{\alpha_c r_A}{\alpha_c r_A + \beta_c r_I} u^{tot}. \quad \text{(Equation 22)}$$

An example simulation showing the input-output map of this module is in Figure 3B, middle panel.

Based on the expressions we just derived, we can qualitatively explain the overall behavior of the BC when the comparator module and the activation/deactivation cycle are interconnected, which is illustrated in the simulation in Figure 3B, right panel. When the input a is smaller than the threshold $k_a(i)$, r_A is almost zero and r_I is large, thereby pushing the value of $\overline{u}$ to approach zero according to Equation 22. In contrast, when a is larger than the threshold $k_a(i)$, r_A is large and r_I is almost zero, therefore $\overline{u}$ approaches u^{tot}. From expression (Equation 22), and from the gain estimatation (Equation 7), it is also apparent that if the switching rate constants α_c and β_c are large, the ultrasensitive response becomes sharper.

Because genetic circuits that implement the BC reactions may be affected by stochastic noise, it is important to ask whether operating near a sharp ultrasensitive threshold may yield a bimodal behavior. Illustrative Gillespie simulations in Section S3.11 indicate that the BC output does not exhibit a bimodal response, nor does it produce fluctuations between the on-off regime; however, the variance of the output increases at the threshold and at low copy numbers (Hooshangi et al., 2005).